

MAGIIICAT I. THE Mg II ABSORBER-GALAXY CATALOG

NIKOLE M. NIELSEN¹, CHRISTOPHER W. CHURCHILL¹, GLENN G. KACPRZAK^{2,3}, AND MICHAEL T. MURPHY²

Accepted for publication in ApJ, September 11, 2013

ABSTRACT

We describe the Mg II Absorber-Galaxy Catalog, MAGIIICAT, a compilation of 182 spectroscopically identified intermediate redshift ($0.07 \leq z \leq 1.1$) galaxies with measurements of Mg II $\lambda\lambda 2796, 2803$ absorption from their circumgalactic medium within projected distances of 200 kpc from background quasars. In this work, we present “isolated” galaxies, which are defined as having no spectroscopically identified galaxy within a projected distance of 100 kpc and a line of sight velocity separation of 500 km s^{-1} . We standardized all galaxy properties to the Λ CDM cosmology and galaxy luminosities, absolute magnitudes, and rest-frame colors to the B - and K -band on the AB system. We present galaxy properties and rest-frame Mg II equivalent width, $W_r(2796)$, versus galaxy redshift. The well-known anti-correlation between $W_r(2796)$ and quasar-galaxy impact parameter, D , is significant to the 8σ level. The mean color of MAGIIICAT galaxies is consistent with an Sbc galaxy for all redshifts. We also present B - and K -band luminosity functions for different $W_r(2796)$ and redshift subsamples: “weak absorbing” [$W_r(2796) < 0.3 \text{ \AA}$], “strong absorbing” [$W_r(2796) \geq 0.3 \text{ \AA}$], low redshift ($z < \langle z \rangle$), and high redshift ($z \geq \langle z \rangle$), where $\langle z \rangle = 0.359$ is the median galaxy redshift. Rest-frame color $B-K$ correlates with M_K at the 8σ level for the whole sample but is driven by the strong absorbing, high redshift subsample (6σ). Using M_K as a proxy for stellar mass and examining the luminosity functions, we infer that in lower stellar mass galaxies, Mg II absorption is preferentially detected in blue galaxies and the absorption is more likely to be weak.

Subject headings: galaxies: halos — quasars: absorption lines

1. INTRODUCTION

Galaxies are known to harbor large, extended reservoirs of gas referred to as the circumgalactic medium (CGM). This region contains the material through which filaments accrete, galactic-scale winds outflow, and merging galaxies are tidally stripped – mechanisms which are critical to the growth and transformation of galaxies given that the CGM harbors a gas mass which may rival that of the galaxy itself (Tumlinson et al. 2011; Stocke et al. 2013; Werk et al. 2013). Additionally, theoretical works have established that the baryons in the CGM depend on the dark matter halo mass and various processes such as stellar and active galactic nucleus feedback (Birnboim & Dekel 2003; Maller & Bullock 2004; Kereš et al. 2005; Dekel & Birnboim 2006; Birnboim et al. 2007; Ocvirk, Pichon, & Teyssier 2008; Kereš et al. 2009; Oppenheimer et al. 2010; Stewart et al. 2011; van de Voort et al. 2011; van de Voort & Schaye 2012). As such, the evolution of galaxies is intimately tied to the origin, processing, and fate of gas in their halos, making studies of the CGM key to understanding galaxy evolution.

Campaigns to study the CGM in absorption at $z \leq 1$ have targeted various ions that probe a range of gas densities and temperatures. For $z < 0.3$, OVI absorption (e.g., Tumlinson et al. 2011; Stocke et al. 2013) traces gas with $n_{\text{H}} \sim 10^{-4} \text{ g cm}^{-3}$ between $T = 10^{4.8} \text{ K}$ (photoionized) and $T = 10^{5.5} \text{ K}$ (collisionally ionized). At $z < 1$, CIV absorption (e.g., Chen et al. 2001a) probes $10^{-2} \leq n_{\text{H}} \leq 10^{-4} \text{ g cm}^{-3}$ gas with temperatures in the range of $\sim 10^{4.6} \text{ K}$ (photoionized) and $\sim 10^{5.0} \text{ K}$ (collisionally ionized). The neutral hydrogen component of the CGM has been observed using Ly α absorption

(e.g., Lanzetta et al. 1995; Chen et al. 2001b; Stocke et al. 2013). However, by far the vast majority of surveys have focused on Mg II absorption (e.g., Bergeron & Boissè 1991; Steidel, Dickinson, & Persson 1994; Churchill et al. 2005; Chen et al. 2010a; Kacprzak et al. 2011b), which samples photoionized CGM gas with $n_{\text{H}} \sim 10^{-1} \text{ g cm}^{-3}$ and $T \sim 10^{4.5} \text{ K}$. Further details of $z < 1$ absorbing gas properties are discussed in Bergeron et al. (1994).

The Mg II $\lambda\lambda 2796, 2803$ absorption doublet is well-suited to studying the processes occurring in the CGM since it is easily observed from the ground in the optical at redshifts $0.1 < z < 2.5$. Mg II traces metal-enriched, low ionization gas over a large range of H I column densities, $16 \lesssim \log N(\text{H I}) \lesssim 22$ (Bergeron & Stasińska 1986; Steidel & Sargent 1992; Churchill et al. 1999, 2000a; Rao & Turnshek 2000; Rigby, Charlton, & Churchill 2002), corresponding to a wide range of environments out to projected distances of $\sim 150 \text{ kpc}$ (Kacprzak et al. 2008; Chen et al. 2010a; Churchill et al. 2013a). Detailed information on the gas kinematics with Mg II have indicated the presence of infalling gas (Kacprzak et al. 2010, 2011b; Ribaud et al. 2011; Stewart et al. 2011; Martin et al. 2012; Rubin et al. 2012; Kacprzak et al. 2012) and outflowing galactic-scale winds (Bouché et al. 2006; Tremonti et al. 2007; Martin & Bouché 2009; Weiner et al. 2009; Chelouche & Bowen 2010; Rubin et al. 2010; Bordoloi et al. 2011; Coil et al. 2011; Bouché et al. 2012; Martin et al. 2012).

The various methods employed for surveys of Mg II absorbing galaxies present challenges in understanding the CGM-galaxy interaction. The largest survey has no more than ~ 80 isolated galaxies, yet some 200 are known. Galaxy absolute photometric properties and quasar-galaxy impact parameters were computed using a variety of cosmological parameters (the accepted cosmology at the time a given survey was pub-

¹ New Mexico State University, Las Cruces, NM 88003
 nnielsen@nmsu.edu

² Swinburne University of Technology, Victoria 3122, Australia

³ Australian Research Council Super Science Fellow

lished), which have changed over the last ~ 20 years. Different observing facilities have been used, resulting in various filter sets. Different magnitude systems were employed. Even the selection methods from survey to survey are diverse, and in some cases different surveys report the same absorber-galaxy pairs, causing duplicates throughout the literature. All these factors result in difficulties when synthesizing the galaxy properties and results between studies.

Motivated by the potential that combining the data from our work and other surveys may further illuminate the CGM-galaxy connection, we have endeavored to assemble a database of the extant works focused on Mg II absorption from the CGM of intermediate redshift galaxies. We aim to provide a large uniform data suite based upon a single cosmological parameter set and to standardize all absolute magnitudes to two filters on the AB system. We consolidate the measurements of given absorber-galaxy pairs duplicated in various works to include the highest-quality data available for each absorber-galaxy pair. Such a compilation holds the promise of yielding higher statistical significance in the already published results, and of providing greater leverage for exploring the dependence of CGM Mg II absorption on various galaxy properties.

In this paper we present the construction of the Mg II Absorber-Galaxy Catalog, MAGII CAT (pronounced magic-cat). We also present the data and general characteristics of the “isolated galaxy” sample. In several works from which the absorber-galaxy pairs were drawn, group galaxies (which we define below) were identified. Since the absorption associated with multi-galaxy pairs may be probing the intragroup medium, or providing a single absorption measurement from the overlap of the circumgalactic medium from more than one galaxy, we defer presentation and analysis of these pairs for future work. Our aim here is to focus on the CGM-galaxy connection for cases in which the data are consistent, to the best of our knowledge, with the absorption arising in the CGM of a single dominant host galaxy. In a future paper, we will present the “group galaxy” subsample of MAGII CAT and will examine the intragroup medium environment.

We also leave further detailed analysis of the CGM-galaxy connection for other papers in this series, e.g., Paper II (Nielsen, Churchill, & Kacprzak 2012), in which we studied the general characteristics of the CGM with galaxy luminosity, color, and redshift, and Paper III (Churchill et al. 2013c), in which we studied the behavior of the CGM with galaxy virial mass. An additional series paper is planned in which we will study the kinematics of the Mg II absorbing CGM. We have also presented additional analysis of the “isolated” galaxy subsample in Kacprzak, Churchill, & Nielsen (2012) and Churchill et al. (2013b).

In § 2 we provide the selection criteria for inclusion of galaxies in the catalog and briefly describe each of the works from which the galaxies are drawn and the various selection methods. In § 3 we detail the galaxy data we obtained and how we standardized various galaxy and absorption properties. We adopt a Λ CDM cosmology ($H_0 = 70 \text{ km s}^{-1} \text{ Mpc}^{-1}$, $\Omega_M = 0.3$, and $\Omega_\Lambda = 0.7$) and report AB absolute magnitudes throughout this paper. In § 4 we present characteristics of the sample, tabulated values for MAGII CAT galaxies, and luminosity functions. We summarize the present work and conclude with the potential of MAGII CAT in § 5. The catalog is available in its entirety in the on-line journal and has been placed on-line at the NMSU Quasar Absorption Line Group

website⁴.

2. CONSTRUCTING MAGII CAT

We compiled a catalog of galaxies with spectroscopic redshifts $0.07 \leq z \leq 1.1$ within a projected distance of $D < 200 \text{ kpc}$ from a background quasar, with known Mg II absorption or an upper limit on absorption less than 0.3 \AA . We chose to include only galaxies with spectroscopic redshifts, excluding galaxies from e.g., Rao et al. (2011) and Bowen & Chelouche (2011), which have photometric redshifts and would have supplied ~ 30 and ~ 10 galaxies to MAGII CAT, respectively. We also limited the sample to galaxies which are not located in group environments (defined in § 2.3) to the limits the data indicate. The galaxies were primarily drawn from the works of Steidel, Dickinson, & Persson (1994), Churchill et al. (1996), Guillemin & Bergeron (1997), Steidel et al. (1997), Chen & Tinker (2008), Barton & Cooke (2009), Chen et al. (2010a), Kacprzak, Murphy, & Churchill (2010), Gauthier & Chen (2011), Kacprzak et al. (2011a,b), and Churchill et al. (2013a).

The galaxy discovery methods employed by the aforementioned surveys range from unbiased volume-limited samples with no *a priori* knowledge of Mg II absorption in the background quasar spectrum (Barton & Cooke 2009; Gauthier & Chen 2011; Kacprzak et al. 2011a), to magnitude-limited samples (Steidel et al. 1997; Kacprzak, Murphy, & Churchill 2010), one with a luminosity scaled maximum projected separation from the quasar sightline (Chen et al. 2010a), and to samples in which galaxies are searched for at the redshifts of known Mg II absorbers (i.e., absorption selected; Bergeron & Boissè 1991; Steidel, Dickinson, & Persson 1994; Guillemin & Bergeron 1997; Chen & Tinker 2008; Gauthier & Chen 2011; Kacprzak et al. 2011b). Some quasar fields have been imaged from the ground only (some with and some without subtraction of the quasar), while others have been imaged at high resolution with the *Hubble Space Telescope* (HST). As such, our compilation comprises a catalog of galaxies with heterogeneous selection methods, and a range of sensitivity in magnitude and impact parameter. Though it may be argued that a complete galaxy sample is indicated by always identifying a galaxy at the redshift of known Mg II absorption (Steidel, Dickinson, & Persson 1994; Steidel 1995), it is inherently difficult to demonstrate completeness unless the quasar fields are systematically surveyed to a uniform magnitude limit and projected separation from the quasar.

2.1. Overview of Surveys

Here we present a brief overview of the previous works included in MAGII CAT.

2.1.1. SDP94

We obtained the data for galaxies presented in Steidel, Dickinson, & Persson (1994) [hereafter SDP94] with $0.3 \leq z \leq 1.0$ (Steidel, private communication). Their sample is “gas cross section-selected,” meaning that the galaxies were selected based on known Mg II absorption with rest-frame equivalent widths $W_r \geq 0.3 \text{ \AA}$ in the spectra of background quasars. Galaxies were searched for starting at

⁴ <http://astronomy.nmsu.edu/cwc/Group/magiccat>

the quasar position and moving outward in angular separation, θ , with most galaxies having an angular separation less than $10''$. Images of the quasar fields were acquired in the R_s band⁵ using the 2.1 m and 4 m telescopes at Kitt Peak National Observatory, as well as the 2.4 m Hiltner telescope at the Michigan-Dartmouth-MIT Observatory. Images in the infrared K_s band were obtained with NICMOS III cameras on the Kitt Peak 4 m Mayall telescope and the Las Campanas Observatory 2.5 m DuPont telescope. Galaxy spectroscopy was conducted using the Lens/Grism Spectrograph and the Kast Double Spectrograph on the Lick Observatory 3 m Shane telescope. Roughly 30% of the galaxies identified by SDP94 do not have spectroscopically confirmed redshifts; we did not include those galaxies. Many of the galaxies from SDP94 were studied more extensively in later works, and are therefore listed under the most recent work.

2.1.2. Steidel-PC

Steidel (private communication) kindly provided the unpublished “interloper” galaxy data briefly discussed as “control fields” in SDP94 and Steidel (1995). These galaxies were targeted because they were not responsible for absorption [to a 5σ upper limit $W_r(2796) < 0.3 \text{ \AA}$] in background quasar spectra during the campaign of SDP94. Galaxy images and spectroscopy were obtained using the same facilities used by SDP94. Later works have obtained HIRES/Keck (Vogt et al. 1994) or UVES/VLT (Dekker et al. 2000) quasar spectra for all galaxies in this sample, therefore the equivalent width limits for these galaxies have been remeasured at the 3σ level by Churchill et al. (2013a) or the present work.

2.1.3. GB97

Studying quasar fields with known MgII absorbers, Guillemin & Bergeron (1997) [hereafter GB97] identified galaxies producing the absorption at $0.07 < z < 1.2$, with $R < 23.5$ and quasar-galaxy angular separations $\theta < 15''$. Imaging in the R band⁶ and galaxy spectroscopy were conducted on the European Southern Observatory 3.5 m telescope using the ESO Faint Object Spectrograph and Camera (hereafter the R -band from this work will be referred to as R_{EFOSC}). We did not include the high redshift *candidate* absorbers from GB97.

2.1.4. Steidel97

Steidel et al. (1997) [hereafter Steidel97] conducted a deep, magnitude-limited study of the overdense galaxy field within $\theta = 50''$ of 3C 336 (1622+238). Galaxies as faint as $R_s = 24.5$ were imaged in R_s with the Michigan-Dartmouth-MIT 2.4 m Hiltner telescope and F702W with WFPC2 on the *Hubble Space Telescope* (*HST*). Infrared K_s band images were obtained with the Kitt Peak 4 m Mayall telescope, with the final image reaching Vega magnitude $K_s \sim 22$ (AB magnitude $K_s \sim 23.8$). Quasar spectra were collected from various instruments and telescopes: the Faint Object Spectrograph on *HST*, the Kast Double Spectrograph with the Lick Observatory 3 m Shane telescope, the RC Spectrograph at the Kitt Peak 4 m Mayall telescope, and the Low Resolution Imaging Spectrograph (LRIS) on the 10 m Keck-I telescope. Galaxy

spectroscopy was conducted with the LRIS/Keck-I combination. The data presented in Steidel97 have been improved upon in later works, in fact a UVES/VLT spectrum is now available, therefore we reference these galaxies according to the work giving updated values, with Steidel97 as the source of the K_s magnitudes.

2.1.5. CT08

Chen & Tinker (2008) [hereafter CT08] selected several quasar fields for which about half of the galaxy data was available from prior MgII surveys (Steidel97), and half from Ly α and CIV surveys (Lanzetta et al. 1995; Chen et al. 1998, 2001a,b). The majority of galaxies were imaged in the F702W band with WFPC2 on *HST*, while galaxies in the field 0226-4110 were imaged in R_f with IMACS on the Magellan Baade telescope. Quasar spectroscopy was obtained with the MIKE Echelle Spectrograph on the Magellan Clay telescope or were obtained from the ESO data archive where they had been observed with UVES on the Very Large Telescope (VLT).

2.1.6. BC09

Working with the Sloan Digital Sky Survey (SDSS) Data Release 4 (DR4) and Data Release 6 (DR6), Barton & Cooke (2009) [hereafter BC09] performed a volume-limited survey of galaxies at $z \sim 0.1$, with a limiting absolute magnitude $M_r \leq -21.3$. Background quasars were selected at projected distances less than or equal to 107 kpc from the galaxies from the SDSS Data Release 6 (DR6) quasar catalog. Galaxy spectra were collected from SDSS while quasar spectra were obtained using the blue channel of LRIS on Keck-I. We obtained apparent SDSS “model” g and r magnitudes from a NASA/IPAC Extragalactic Database (NED)⁷ search. The equivalent widths for several of these galaxies were remeasured by Kacprzak et al. (2011a).

2.1.7. Chen10

Chen et al. (2010a) [hereafter Chen10] photometrically selected galaxies with $z < 0.5$ from the SDSS DR6 archive with $r' < 22$. Galaxies in quasar fields were targeted with the limitation that the quasar-galaxy impact parameter, D , must be less than the expected gaseous radius for each galaxy, $R = R_*(L_B/L_B^*)^{0.35}$, where $R_* = 130$ kpc. Follow up galaxy and quasar spectroscopy was obtained using the Dual Imaging Spectrograph (DIS) on the 3.5 m telescope at the Apache Point Observatory (APO) or with MagE on the Magellan Clay Telescope at the Las Campanas Observatory. We obtained apparent SDSS model g and r magnitudes from NED. The published $W_r(2796)$ upper limits were converted from 2σ to 3σ upper limits and we included only those galaxies for which the upper limit was less than or equal to 0.3 \AA .

2.1.8. KMC10

Performing a magnitude-limited survey down to $F814W \leq 20.3$, Kacprzak, Murphy, & Churchill (2010) [hereafter KMC10] studied the field 1127-145 which contains many bright galaxies within an angular quasar-galaxy separation of $50''$. The field was imaged in the F814W band on *HST* with WFPC2. Spectroscopy of the galaxies was obtained with DIS at the APO 3.5 m telescope, while quasar spectroscopy was conducted with UVES/VLT.

⁵ Chuck Steidel kindly provided the electronic versions of the R_s and K_s filter response curves.

⁶ The electronic version of the ESO Faint Object Spectrograph and Camera R filter response curve was kindly provided by Jacqueline Bergeron.

⁷ <http://ned.ipac.caltech.edu>

2.1.9. *GC11*

Gauthier & Chen (2011) [hereafter GC11] studied luminous red galaxies (LRGs) that were photometrically identified in SDSS DR4 with $z \approx 0.5$ and a maximum D corresponding to the fiducial virial radius of LRGs, which is given as 500 kpc. A subset of their LRGs were selected by known Mg II absorbers in quasar spectra, while a larger subset was randomly selected near quasar sightlines with no prior knowledge of Mg II absorption. Galaxy spectra were obtained using DIS on the 3.5 m telescope at APO or with the Boller & Chivens Spectrograph on the Las Campanas DuPont telescope. We obtained apparent SDSS “model” g and r magnitudes from NED and included only those LRGs with impact parameters $D < 200$ kpc in MAGII CAT. We also converted the published upper limits on $W_r(2796)$ from 2σ to 3σ , including only those galaxies with $W_{\text{lim}} \leq 0.3 \text{ \AA}$.

2.1.10. *KCBC11*

Kacprzak et al. (2011a) [hereafter KCBC11] built upon the work of BC09 by adding galaxies of somewhat larger redshift, $z \sim 0.13$. Galaxy spectra were obtained with DIS on the 3.5 m APO telescope, while quasar spectra were collected using the blue channel of LRIS on Keck-I. Using NED, we obtained the SDSS “model” r and 2MASS total K_s apparent magnitudes for all but two galaxies, where K_s was not available. We instead obtained the SDSS “model” g and r magnitudes for those two galaxies.

2.1.11. *KCEMS11*

Galaxies selected by Kacprzak et al. (2011b) [hereafter KCEMS11] are based on known Mg II absorption at $0.3 < z < 1$ in quasar spectra, with many having been originally identified by SDP94. Imaging of the quasar fields was conducted by *HST* with the F702W or F814W filters on WFPC2. Infrared imaging for the SDP94 fields was conducted in the K_s band with the NICMOS III cameras on the Kitt Peak 4 m Mayall telescope and the Las Campanas Observatory 2.5 m DuPont telescope. K' magnitudes were obtained for three galaxies from Chen et al. (2001b), who used NSFCAM on the IRTF 3 m telescope, and F160W magnitudes for two galaxies from David Law (private communication) who observed them with WFC3 on *HST*. Quasar spectroscopy was obtained with HIRES/Keck or UVES/VLT, while galaxy spectroscopic redshifts were collected from the literature (see Table 3 in KCEMS11).

2.1.12. *Churchill13*

Requiring high resolution quasar spectra ($R = 45,000$) and *HST* images, Churchill et al. (2013a) [hereafter Churchill13] studied galaxies with weak [$W_r(2796) < 0.3 \text{ \AA}$] or undetected Mg II absorption. Half of the galaxies in this sample were obtained from Steidel-PC, while the other half were collected from Steidel97, Churchill et al. (2007), CT08, and KMC10. Galaxies were imaged in F702W or F814W with WFPC2 on *HST* and, in some cases, in K_s as detailed in Steidel-PC. Quasar spectra were obtained with HIRES/Keck, UVES/VLT, or with the MIKE Echelle Spectrograph on the Magellan Clay telescope. We included galaxies listed as the “New Sample” in Table 2 in Churchill13.

2.2. *Sources of Data*

In Table 1, we present the sources of data for galaxies in MAGII CAT. We present the work from which galaxies were

TABLE 1
SOURCES OF DATA IN MAGII CAT^a

(1) Survey	(2) Galaxy ID	Magnitudes		Absorption		
		(3) B	(4) K	(5) $W_r(2796)$	(6) Absorbers	(7) Upper Limits
GB97	9	9	0	3	3	0
Churchill13	18	17	9	20	0	20
KCEMS11	33	33	0	32	32	0
Steidel97	0	0	11	0	0	0
CT08	5	5	0	3	2	1
Chen10	68	0	0	68	47	21
SDP94	18	18	38	7	7	0
Steidel-PC	0	1	1	0	0	0
KMC10	4	4	0	1	0	1
KCBC11	9	0	0	9	9	0
GC11	12	0	0	12	5	7
BC09	6	0	0	6	0	6
This Work	0	95	105	21	18	3
Total	182	182	164	182	123	59

^a The numbers associated with each “survey” reflect the source from which the data we published are taken. In cases where a “0” appears, this is because all of the galaxy or absorption data was either published elsewhere for the first time or republished with higher quality data in a later work.

obtained in column (1). The rest of the columns contain the number of galaxies for which the following data was obtained: (2) the galaxy identification, such as redshift and impact parameter, (3) the observed magnitude used to calculate the B -band absolute magnitude, (4) the observed magnitude used to calculate the K -band absolute magnitude, and (5) the Mg II equivalent width, while columns (6) and (7) contain the number of galaxies that have detectable absorption and have an upper limit on absorption, respectively.

We note that for many of the sources from which data were obtained, the images of the quasar fields were not published. In cases in which images were published and/or annotated, we did not have access to the electronic data in order to verify and/or directly characterize the magnitude limits and galaxy detection thresholds. As such, we have not been able to directly inspect the imaged fields around the quasars for a substantial portion of the sample. In addition, in many cases the spectra showing the Mg II absorption lines were not published so that we have had to rely upon the published equivalent width measurements.

2.3. *Defining Isolated and Group Galaxies*

In this paper, we present only “isolated” galaxies since we are focused on the CGM of individual systems. We define an isolated galaxy to be one in which there is no spectroscopically identified galaxy within 100 kpc (projected) and a line of sight velocity separation of 500 km s^{-1} . Conversely, a group galaxy is defined to have a spectroscopically identified nearest neighbor within a projected separation of 100 kpc and having a line of sight relative velocity less than 500 km s^{-1} . This definition is adopted from Chen et al. (2010a), but modified to include a slightly larger velocity separation.

Since we are unable to examine all images of the quasar fields to search for faint objects near the quasar or the identified absorbing galaxy, we cannot place more stringent limits on the definition separating isolated and group galaxies.

In the following section, we present an averaged relationship between limiting absolute magnitude and limiting apparent magnitude based upon the general specifications of the published surveys (see Figures 4a and 4b). The curves show that the “average” survey is generally not deep enough to extend down to luminous satellites like the Large Magellanic Cloud around the Milky Way, and certainly cannot detect dwarf galaxies in groups. Thus, the definition of isolated and group galaxies refers, on average, to the brighter galaxy population.

Our ability to distinguish a group such as the Local Group based upon its brightest members, M31 and the Milky Way, is, in the end, dependent upon the direction from which the the Local Group would be viewed. Given the ~ 700 kpc distance between M31 and the Milky Way, a line of sight perpendicular to their separation vector would render both galaxies as isolated regardless of their relative sightline velocities. On the other hand, a line of sight more or less parallel to their separation vector in which their projected separation is less than 100 kpc would render their being classified as group galaxies, given that their line of sight velocity separation is on the order of $\sim 400 \text{ km s}^{-1}$. As such, there is likely some level, which is difficult to quantify, to which the isolated sample contains galaxies in environments similar to the Local Group. And, for those galaxies classified as group members, there may be some fraction for which the galaxies are physically separated by a large enough distance that their respective CGM environments do not overlap into an intragroup medium (which is likely the case for M31 and the Milky Way, but would in general depend upon the dynamical history of the group).

As we stated above, we present only isolated galaxies in this paper drawing upon a definition set by precedent in the literature. The intragroup medium of the group galaxy subsample will be studied in a forthcoming paper.

3. METHODS

For each galaxy, the measured quantities include one or more apparent magnitudes in various photometric bands, the spectroscopic redshift, z_{gal} , the galaxy right ascension and declination offsets from the quasar, $\Delta\alpha$ and $\Delta\delta$, and/or the galaxy angular separation from the quasar, θ . Many of the galaxies have multiple measurements from several different studies; we selected the highest quality measurements (usually the most recent).

3.1. Galaxy Properties

Galaxy redshifts, z_{gal} , were taken directly from published values. The galaxy spectra were not published in most cases and were not available in electronic form for further confirmation or re-measurement. Since the uncertainties of z_{gal} were also not published, the accuracy of the published z_{gal} measurements is reflected by the number of significant figures.

Due to the application of different cosmologies in the literature over the last ~ 20 years, we calculated new impact parameters, D , and luminous properties for each galaxy using the Λ CDM cosmology ($H_0 = 70 \text{ km s}^{-1} \text{ Mpc}^{-1}$, $\Omega_M = 0.3$, and $\Omega_\Lambda = 0.7$).

We first calculated the values $\Delta\alpha$ and $\Delta\delta$ from the right ascensions and declinations of the galaxy and its associated quasar, which were obtained from NED when available. We then determined θ from $\Delta\alpha$ and $\Delta\delta$ using $\theta = [(\Delta\delta)^2 + (\Delta\alpha)^2 \cos^2(\delta_{\text{QSO}})]^{1/2}$. We compute the impact parameter from $D = \theta D_A(z_{\text{gal}})$, where $D_A(z_{\text{gal}})$ is the angular di-

ameter distance at the galaxy redshift. In cases where $\Delta\alpha$ and $\Delta\delta$ could not be obtained, we used the published values of θ to calculate D . Using these methods, we have measured $\Delta\alpha$ and $\Delta\delta$ for most galaxies and standardized impact parameters for all galaxies in MAGIICAT.

All galaxies have been imaged in the g , r , R_{FOSC} , R_s , R_i , F702W, or F814W bands. For each galaxy, we determined rest-frame AB absolute B -band magnitudes, M_B , using the equation, $M_B(\text{AB}) = [m_y - K_{B_y}] - DM$, where m_y is the AB apparent magnitude in the observed band, K_{B_y} is the appropriate K -correction (e.g., Kim, Goobar, & Perlmutter 1996, see Appendix A) for the observed magnitude, and DM is the distance modulus for each galaxy. In cases where m_y is a Vega magnitude, such as F702W and F814W, we add the constant -0.0873 to convert from Vega magnitudes to AB magnitudes. Details on how we determined this constant are given in Appendix A.

To compute the K -corrections, we applied the actual filter response curve for each published apparent magnitude. The K -corrections as a function of redshift for the F702W- and g -band to the B -band are shown in panels *a* and *c* of Figure A1, respectively. Using the spectral energy distribution (SED) templates from Bolzonella et al. (2000) who extended the Coleman et al. (1980) SEDs to shorter and longer wavelengths, we adopted a SED for each galaxy. To do this, we compared the observed color of each SED to each galaxy’s observed color and chose the SED with the closest color. For 18 galaxies where no observed galaxy color was available, we adopted an Sbc galaxy SED, the average type selected by MgII absorption (SDP94; Zibetti et al. 2007). Figure B1 in Appendix B presents F702W- K_s and $g-r$, the two most common observed galaxy colors in MAGIICAT, as a function of redshift.

The apparent magnitudes in MAGIICAT have not been Galactic reddening corrected to the extent of our knowledge. We did not apply this correction to the magnitudes as the mean reddening correction in each magnitude band is, on average, a small fraction of the uncertainty in the K -corrections due to SED selections. The greatest reddening correction in MAGIICAT would be applied to the g band, as it is the band measuring the shortest wavelengths. The mean reddening correction in this band is 0.2 magnitudes, while the greatest difference in the K -correction $K_{B,g}$ between an E and an Im SED is 1.5 magnitudes (see Figure A1).

Galaxies drawn from SDP94 and Steidel97 were imaged in the infrared with the K_s band. Many galaxies in CT08, BC09, KCBC10, KCEMS11, and Churchill13 were imaged in either the 2MASS K_s band and obtained from NED, the K' band from Chen et al. (2001b), or the *HST* F160W band from David Law (private communication). Using these values, we computed $M_K(\text{AB})$ from K -corrected infrared magnitudes using the methods applied for the B -band and the equation, $M_K(\text{AB}) = [m_y - K_{K_y}] - DM + 1.8266$, where m_y is the Vega apparent magnitude and the value 1.8266 is the constant used to convert from Vega magnitudes to AB magnitudes in all cases. The K -corrections in the K_s band for each SED are presented in panel *b* of Figure A1 as a function of redshift.

Apparent magnitudes in the K -band were not available for all galaxies drawn from Chen10 and GC11, and many galaxies from BC09 and KCBC11. We used an indirect method to compute M_K by determining rest-frame $B-K$ colors from rest-frame $B-R$ colors. We obtained “model” g and r apparent magnitudes from NED/SDSS. We adopt “model” magnitudes because the galaxy light is measured consistently through the

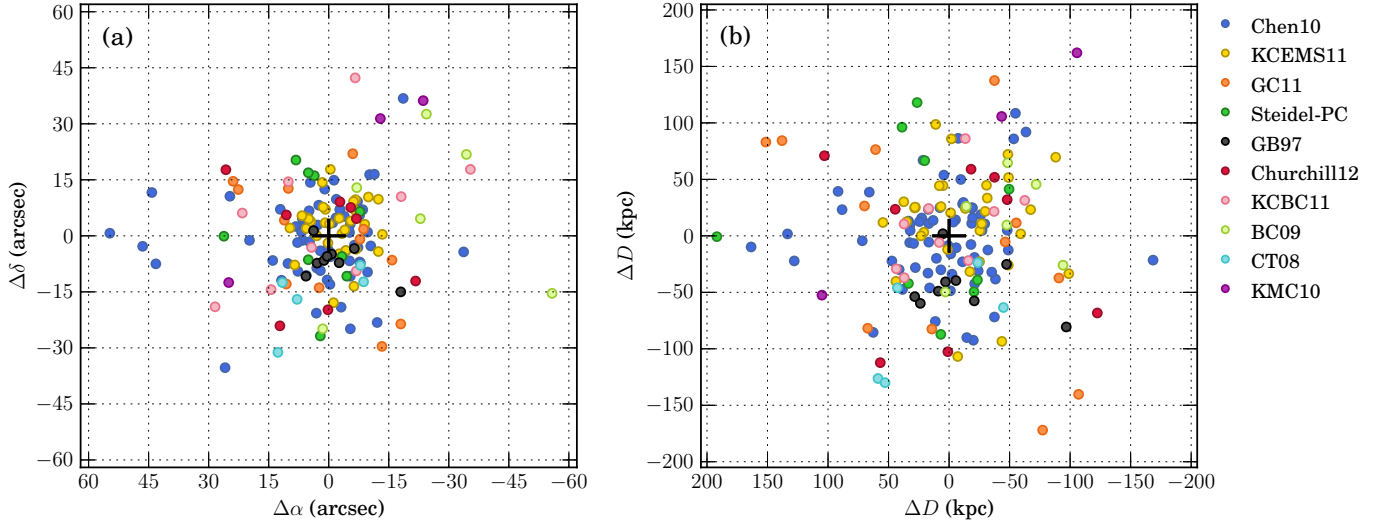


FIG. 1.— (a) Angular offsets (arcsec) of each galaxy for which we have $\Delta\alpha$ and $\Delta\delta$ from the associated background quasar. (b) Physical offsets (kpc) of each galaxy from the associated background quasar. Points are color coded by the work from which the galaxy was obtained. The plus sign indicates the location of the background quasar.

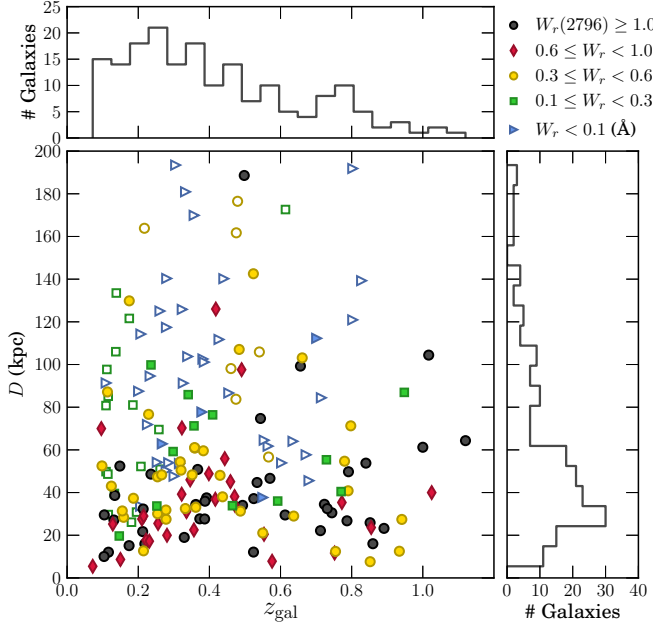


FIG. 2.— The quasar-galaxy impact parameter, D , as a function of galaxy redshift, z_{gal} . Points are colored by $W_r(2796)$, with open points representing 3σ upper limits on $W_r(2796)$. Open yellow circles indicate galaxies with an upper limit of $W_r(2796) = 0.3$ Å, the largest upper limit in MAG11CAT. Histograms show the distribution of D and z_{gal} for the full sample.

same aperture in all bands, therefore they are the best magnitudes for measuring the colors of galaxies. Using these magnitudes and the methods for M_B above, we calculated M_B from g and M_R from r . The K -corrections for these magnitudes are presented in panels *c* and *d* of Figure A1, respectively. In order to convert these $B-R$ colors to $B-K$, we computed rest-frame $B-R$ and $B-K$ colors for each galaxy SED, which suggest a linear relationship with the form $(B-K) = 1.86(B-R) + 0.02$, determined from a linear least-squares fit to the rest-frame SED colors. The rest-frame colors of each SED and the linear fit are presented in Figure C1. We then applied this relation to the $B-R$ colors to obtain $B-K$. Finally,

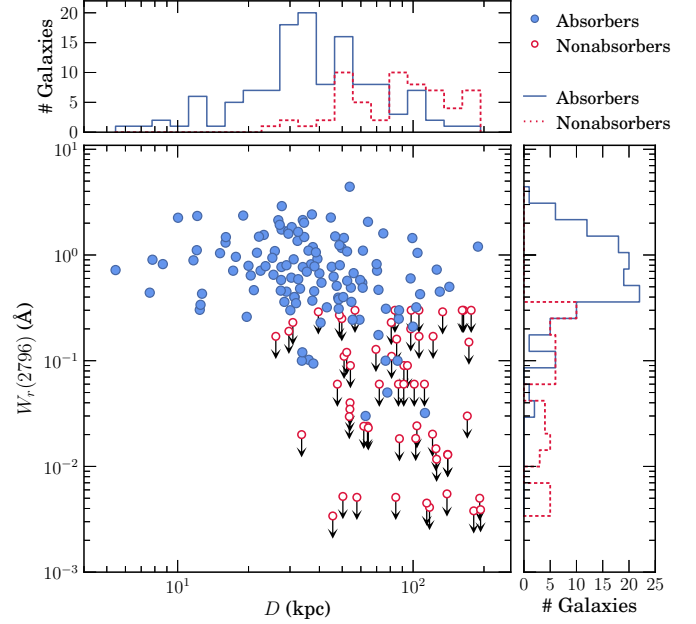


FIG. 3.— The rest-frame MgII equivalent width, $W_r(2796)$, versus impact parameter, D . Points are colored based on $W_r(2796)$ absorption, with solid blue points representing galaxies with measured absorption and red open points with downward arrows representing 3σ upper limits on $W_r(2796)$. The histograms show the D and $W_r(2796)$ distributions for absorbers (thin blue line) and an upper limit on absorption (dotted red line). The anti-correlation between $W_r(2796)$ and D is significant at the 7.9σ level.

M_K was calculated from M_B and $B-K$. Using these methods, we obtained colors for all but 18 galaxies in MAG11CAT.

B -band luminosities, L_B/L_B^* , were obtained using a linear fit to M_B^* with redshift using the “All” sample in Table 6 from Faber et al. (2007). The K -band luminosities, L_K/L_K^* , were computed using $M_K^*(z)$ as expressed in Eq. 2 from Cirasuolo et al. (2010).

3.2. Absorption Properties

Where we have obtained access to HIRES/Keck or UVES/VLT quasar spectra, we have remeasured $W_r(2796)$ us-

TABLE 2
 OBSERVED GALAXY PROPERTIES^a

(1) QSO	(2) J-Name	(3) z_{gal}	Galaxy ID				B-band			K-band			(14) SED ^f
			(4) $\Delta\alpha$ (arcsec)	(5) $\Delta\delta$ (arcsec)	(6) θ (arcsec)	(7) Ref ^b	(8) m_y ^c	(9) Band ^d	(10) Ref ^b	(11) m_y ^e	(12) Band ^d	(13) Ref ^b	
0002-422	J000448.11-415728.8	0.840	-6.4	-3.4	7.10	1	22.60	$R_{\text{EFOSC}}(\text{V})$	1	(Sbc)
0002+051	J000520.21+052411.80	0.298	-13.4	0.4	13.45	3	19.86	F702W(V)	3	16.37	$K_s(\text{V})$	7	E/S0
0002+051	J000520.21+052411.80	0.592	-2.6	-4.8	5.46	3	21.11	F702W(V)	3	17.40	$K_s(\text{V})$	7	E/S0
0002+051	J000520.21+052411.80	0.85180	-3.3	0.6	3.40	3	22.21	F702W(V)	3	19.30	$K_s(\text{V})$	7	Im
SDSS	J003340.21-005525.53	0.2124	-5.4	3.2	6.28	6	19.44	$g(\text{AB})$	14	18.79	$r(\text{AB})$	14	Scd
SDSS	J003407.34-085452.07	0.3617	6.5	-1.2	6.56	6	22.41	$g(\text{AB})$	14	21.45	$r(\text{AB})$	14	Scd
SDSS	J003413.04-010026.86	0.2564	-2.8	7.1	7.63	6	21.68	$g(\text{AB})$	14	20.25	$r(\text{AB})$	14	E/S0
0058+019	J010054.15+021136.52	0.6128	4.40	7	23.25	$R_s(\text{AB})$	7	19.90	$K_s(\text{V})$	7	Sbc
0058+019	J010054.15+021136.52	0.680	-3.3	-5.5	6.50	2	22.06	F702W(V)	2	18.65	$K_s(\text{V})$	8	Sbc
SDSS	J010135.84-005009.08	0.2615	10.2	-7.4	12.60	6	20.91	$g(\text{AB})$	14	19.57	$r(\text{AB})$	14	E/S0

^a Table 2 is published in its entirety in the electronic edition of ApJ. A portion is shown here for guidance regarding its form and content.

^b Galaxy Identification and Apparent Magnitude Reference: (1) Guillemin & Bergeron (1997), (2) Churchill et al. (2013a), (3) Kacprzak et al. (2011b), (4) Steidel et al. (1997), (5) Chen & Tinker (2008), (6) Chen et al. (2010a), (7) Steidel, Dickinson, & Persson (1994), (8) Steidel-PC, (9) Kacprzak, Murphy, & Churchill (2010), (10) Kacprzak et al. (2011a), (11) Gauthier & Chen (2011), (12) Barton & Cooke (2009), (13) Chen et al. (2001b), (14) NED/SDSS, (15) NED/2MASS, and (16) David Law, personal communication.

^c Apparent magnitude used to obtain M_B .

^d Magnitude Band and Type: (AB) AB magnitude, and (V) Vega magnitude.

^e Apparent magnitude used to obtain M_K .

^f Galaxy Spectral Energy Distributions: (Sbc) No color information – Sbc used.

ing the methods of Schneider et al. (1993) and Churchill et al. (2000a). Upper limits on $W_r(2796)$ are quoted at 3σ and must be less than or equal to 0.3 \AA , corresponding to an unresolved absorption feature, for a galaxy to be included in MAGIIICAT. In cases where HIRES/Keck and/or UVES/VLT spectra do not exist, we adopted the best published values. In most cases, these are measurements are take directly from tabulated data. We have also converted published 2σ upper limits to 3σ where needed. We have not included galaxies with upper limits less stringent than 0.3 \AA in order to ensure all non-detections reside below the historical absorption threshold of 0.3 \AA (SDP94).

Adopting a 3σ upper limit of $W_r(2796) = 0.3\text{ \AA}$ allows us to distinguish two subsamples by absorption strength based upon historical precedence. Several of the surveys from which MAGIIICAT is constructed were conducted on 4-meter class telescopes using moderate resolution ($\sim 1\text{ \AA}$); the typical equivalent width detection sensitivity of these surveys was $W_r(2796) = 0.3\text{ \AA}$. Not until the advent of the HIRES spectrograph on Keck I in the early 1990s was it possible to systematically explore equivalent widths below this threshold (Churchill et al. 1999). Absorbers with $W_r(2796) < 0.3\text{ \AA}$ were thus dubbed “weak systems”.

Following the historical precedent, we adopt the term “strong” absorption for values in the range $W_r(2796) \geq 0.3\text{ \AA}$. However, we note that this term has often been applied in the literature to describe absorbers with $W_r(2796) \geq 1.0\text{ \AA}$ or higher. Throughout this work, we also adopt the term “weak” absorption for values in the range $W_r(2796) < 0.3\text{ \AA}$, regardless of whether absorption was formally detected or not detected to the varying limits of the HIRES and/or UVES quasar spectra.

The term “non-absorber” is most suitably applied for surveys designed to be complete to a well-defined detection threshold, in which upper limits below the threshold would be described using such a term to indicate “below the sur-

vey limit”. In a global description of absorption strengths, we must keep in mind that a non-detection does not provide evidence for no absorption. A highly stringent limit on $W_r(2796)$ could indicate that the line of sight passed through a low-density, high-ionization region in which the ionization fraction of Mg II is vanishingly small. Similarly, it could indicate that the line of sight probed a very low H I column density, dense, low-ionization structure, such that even with a high metallicity and a high ionization fraction, Mg II would not be detected to the limits of the data. It is likely extremely rare that gas within 200 kpc (projected) of a galaxy and relative velocity within a few hundred kilometers per second would be entirely devoid of Mg II absorption.

In order to simplify terminology, we adopt the two terms “weak” and “strong” absorption, and remind the reader that “weak” absorption encompasses all measurements below $W_r(2796) = 0.3\text{ \AA}$ and all upper limits, since presumably higher and higher sensitivities would yield “detections” in most all cases.

4. GALAXY SAMPLE

Here we present basic characteristics of MAGIIICAT, leaving any analysis to future work.

MAGIIICAT consists of 182 isolated galaxies along 134 sightlines. The redshift range of the sample is $0.07 \leq z \leq 1.12$, with median $\langle z \rangle = 0.359$.

Observed galaxy properties for MAGIIICAT are presented in Table 2. The columns include the (1) QSO identifier, (2) Julian 2000 designation (J-Name), (3) galaxy spectroscopic redshift, z_{gal} , (4) quasar-galaxy right ascension offset, $\Delta\alpha$, (5) quasar-galaxy declination offset, $\Delta\delta$, (6) quasar-galaxy angular separation, θ , (7) reference for columns 4, 5, and 6, (8) apparent magnitude used to obtain M_B , (9) band for the preceding apparent magnitude, (10) reference for columns 8 and 9, (11) apparent magnitude used to calculate M_K , (12) band for m_K , (13) reference for columns 11 and 12, and (14) galaxy spectral energy distribution type based on the galaxy observed

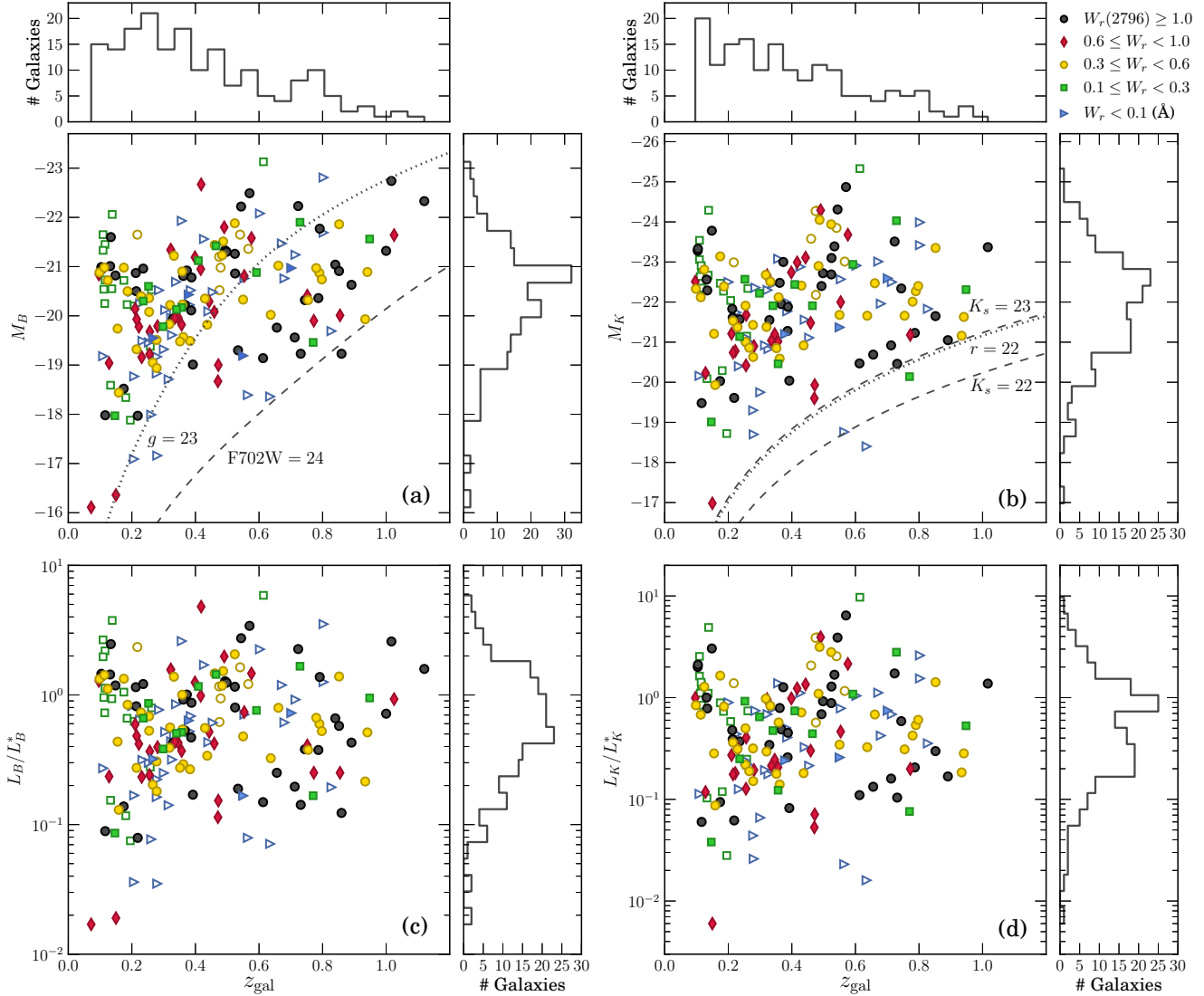


FIG. 4.— Galaxy luminous properties, M_B , M_K , L_B/L_B^* , and L_K/L_K^* , as a function of redshift. Point types indicate the strength of Mg II absorption, $W_r(2796)$. Open points represent upper limits on absorption. The distributions of redshift and luminous properties are shown in histograms along the respective axes. (a) The B -band AB absolute magnitude, M_B , as a function of galaxy redshift, z_{gal} . M_B is calculated at all redshifts from apparent magnitudes of $g = 23$ (AB magnitude; dotted line) and F702W = 24 (Vega magnitude; dashed line), representing the limiting magnitudes for the surveys in which many of the galaxies were observed. The value of g comes from the Sloan Digital Sky Survey, whereas the F702W-band was observed with WFPC2 on *HST*. (b) The K -band AB absolute magnitude, M_K , versus galaxy redshift, z_{gal} . M_K is calculated at all redshifts from apparent K_s - and r -band magnitudes to indicate the limiting magnitudes associated with the various samples in MAGIICAT. The majority of galaxies imaged with the K_s -band have a limiting magnitude of $K_s = 21$ (Vega magnitude; dashed line), while those obtained from Steidel97 were imaged more deeply down to $K_s = 22$ (Vega magnitude; dashed line). Galaxies imaged in the r -band with SDSS have a limiting magnitude of $r = 22$ (dotted line). We translated M_r into M_K using the relationship between $B-R$ and $B-K$ colors in § 3.1 and Appendix C. (c) The B -band luminosity, L_B/L_B^* , as a function of galaxy redshift, z_{gal} . (d) The K -band luminosity, L_K/L_K^* , versus galaxy redshift, z_{gal} .

color.

The galaxy right ascension and declination offsets from the quasar, $\Delta\alpha$ and $\Delta\delta$, are presented in Figure 1a. Points are colored by reference, indicating the work from which the galaxy data was drawn. No values for $\Delta\alpha$ and $\Delta\delta$ were originally published for galaxies from SDP94, though later works have obtained the values for many of these galaxies (Steidel, private communication). The plus sign indicates the location of the associated background quasar.

Figure 1b shows the location of each galaxy in MAGIICAT in physical units (kpc) with respect to the associated background quasar (plus sign). The points are colored by the source of the $\Delta\alpha$ and $\Delta\delta$ measurements.

Impact parameter, D , as a function of galaxy redshift, z_{gal} ,

is presented in Figure 2. Points are colored by $W_r(2796)$, with 3σ upper limits on $W_r(2796)$ represented as open points. Histograms of the data collapsed along the axes show the distribution of impact parameters and galaxy redshifts. Impact parameters range from $5.4 \leq D \leq 194$ kpc, where the median impact parameter is $\langle D \rangle = 48.7$ kpc.

From Figure 2, it is apparent that most galaxies with upper limits on absorption are found at larger impact parameters. This anti-correlation between $W_r(2796)$ and D is a commonly known property of Mg II galaxies (e.g., Lanzetta & Bowen 1990; Bergeron & Boissé 1991; Steidel 1995; Bouché et al. 2006; Kacprzak et al. 2008; Chen et al. 2010a; Churchill et al. 2013a). We performed a non-parametric Kendall's τ rank correlation test on $W_r(2796)$

TABLE 3
CALCULATED GALAXY AND ABSORPTION PROPERTIES ^a

(1) QSO	(2) J-Name	(3) z_{gal}	Mg II Absorption				(8) D (kpc)	B -band			K -band			(15) $B-K$
			(4) z_{abs}	(5) $W_r(2796)$ Å	(6) DR	(7) Ref ^b		(9) K_{By} ^c	(10) M_B ^d	(11) L_B/L_B^*	(12) K_{Ky} ^e	(13) M_K ^d	(14) L_K/L_K^*	
0002-422	J000448.11-415728.8	0.840	0.836627	4.422 ± 0.002	1.12 ± 0.09	13	53.8	-0.08	-21.04	0.66
0002+051	J000520.21+052411.80	0.298	0.298059	0.244 ± 0.003	1.336 ± 0.029	3	59.2	-1.39	-19.78	0.38	-0.52	-22.22	0.64	2.43
0002+051	J000520.21+052411.80	0.592	0.591365	0.102 ± 0.002	1.539 ± 0.039	3	36.0	-0.80	-20.88	0.76	-0.53	-22.94	1.08	2.05
0002+051	J000520.21+052411.80	0.85180	0.851393	1.089 ± 0.008	1.160 ± 0.013	3	25.9	-0.64	-20.91	0.58	-0.88	-21.65	0.29	0.74
SDSS	J003340.21-005525.53	0.2124	0.2121	1.05 ± 0.03	...	6	21.7	0.20	-20.87	1.15	0.06	-21.83	0.47	0.96
SDSS	J003407.34-085452.07	0.3617	0.3616	0.48 ± 0.05	...	6	33.1	0.54	-19.57	0.29	0.13	-20.59	0.14	1.02
SDSS	J003413.04-010026.86	0.2564	0.2564	0.61 ± 0.06	...	6	30.4	0.80	-19.68	0.37	0.43	-21.68	0.40	1.99
0058+019	J010054.15+021136.52	0.6128	0.612586	1.684 ± 0.004	1.06 ± 0.09	13	29.5	-0.40	-19.14	0.15	-0.59	-20.47	0.11	1.32
0058+019	J010054.15+021136.52	0.680	0.680	< 0.0034	...	2	45.6	-0.34	-20.76	0.61	-0.63	-21.96	0.42	1.20
SDSS	J010135.84-005009.08	0.2615	0.2615	< 0.11	...	6	50.9	0.82	-20.53	0.80	0.44	-22.34	0.74	1.81

^a Table 3 is published in its entirety in the electronic edition of ApJ. A portion is shown here for guidance regarding its form and content.

^b Mg II Absorption Measurements: (1) Guillemin & Bergeron (1997), (2) Churchill et al. (2013a), (3) Kacprzak et al. (2011b), (4) Steidel et al. (1997), (5) Chen & Tinker (2008), (6) Chen et al. (2010a), (7) Steidel, Dickinson, & Persson (1994), (8) Steidel-PC, (9) Kacprzak, Murphy, & Churchill (2010), (10) Kacprzak et al. (2011a), (11) Gauthier & Chen (2011), (12) Barton & Cooke (2009), (13) Evans (2011), and (14) This work.

^c K -correction used to obtain M_B from column (8) in Table 2.

^d Absolute magnitudes are AB magnitudes.

^e K -correction used to obtain M_K from column (11) in Table 2.

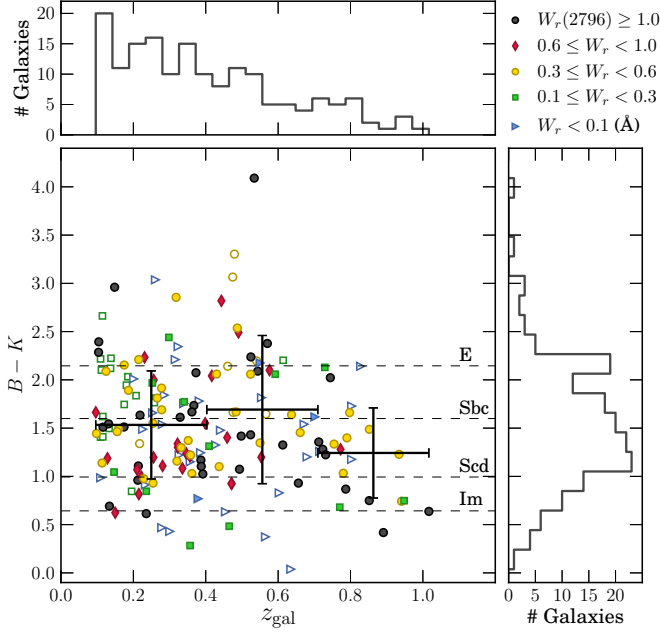


FIG. 5.— Rest-frame galaxy color, $B-K$, against galaxy redshift, z_{gal} . Points are colored by $W_r(2796)$, with open points representing upper limits on $W_r(2796)$. The dashed lines mark the rest-frame $B-K$ colors for the spectral energy distributions of E, Sbc, Scd, and Im galaxies. Crosses indicate the average color in three redshift bins ($z < 0.403$, $0.403 \leq z < 0.709$, and $z \geq 0.709$). Horizontal error bars show the range in redshift for each bin while vertical error bars are the standard deviations in $B-K$ for each bin. The average colors in all three redshift bins are consistent with an Sbc galaxy. Color and redshift distributions for MAGIIICAT are presented as histograms. From the color histogram, the most common galaxy type is slightly redder than an Scd galaxy.

and D , allowing for upper limits on $W_r(2796)$ (see Brown, Hollander, & Korwar 1974; Wang & Wells 2000). We find that $W_r(2796)$ is anti-correlated with D at the 7.9σ level. We present the anti-correlation in Figure 3, leaving any analysis for future work in which we explore the scatter in the relationship as a function of galaxy properties (see Paper II and Churchill et al. 2013b). Galaxies with measured absorption are shown as blue points, while upper limits on absorption are open red circles with downward arrows. The distributions of $W_r(2796)$ and D for absorbers (thin blue lines), and galaxies with upper limits on absorption (dotted red lines) are presented in histograms.

The equivalent width detections and upper limits on absorption of MAGIIICAT galaxies have a range of $0.003 \leq W_r(2796) \leq 4.42 \text{ \AA}$, where the weakest confirmed absorption is $W_r(2796) = 0.03 \text{ \AA}$. Of the 182 galaxies, 59 have upper limits on $W_r(2796)$ where the most stringent upper limit is 3 m\AA . To a 3σ $W_r(2796)$ threshold, MAGIIICAT is 100% complete to 0.3 \AA , 90% complete to 0.2 \AA , 80% complete to 0.05 \AA , and 70% complete to 0.01 \AA .

The absolute B -band magnitudes range from $-16.1 \geq M_B \geq -23.1$. Figure 4a shows M_B as a function of z_{gal} . Points are colored by $W_r(2796)$, with open points representing upper limits on $W_r(2796)$. Histograms show the distribution of galaxies in redshift and M_B .

Absolute K -band magnitudes range from $-17.0 \geq M_K \geq -25.3$. Figure 4b presents M_K against z_{gal} . Points are colored by $W_r(2796)$, with upper limits on $W_r(2796)$ shown as open points. Histograms present the distribution of redshift

TABLE 4
MAGIIICAT PROPERTIES

Property	Min	Max	Mean	Median
$W_r(2796) (\text{\AA})$	0.003	4.422	0.629	0.400
z_{gal}	0.072	1.120	0.418	0.359
$D (\text{kpc})$	5.4	193.5	61.1	48.7
M_B	-16.1	-23.1	-20.3	-20.4
M_K	-17.0	-25.3	-21.9	-22.0
L_B/L_B^*	0.017	5.869	0.855	0.611
L_K/L_K^*	0.006	9.712	0.883	0.493
$B-K$	0.04	4.09	1.54	1.48

and M_K of the sample.

The completeness limits of the magnitudes are complicated due to the heterogeneous imaging campaigns described in § 2.1. For the B -band, the majority of galaxies at low redshift ($z < \langle z \rangle$, where $\langle z \rangle = 0.359$ is the median redshift of the sample) were selected by SDSS r magnitudes with a limiting magnitude of $r = 22$. However, we used the SDSS g band for these galaxies to calculate M_B , which is sensitive to the threshold $g \simeq 23$ (AB magnitude; dotted line in Figure 4a). At the mean redshift of the low redshift subsample, $z = 0.23$, this corresponds to $M_B \simeq -17.5$. The majority of galaxies at high redshift ($z \geq \langle z \rangle$) were imaged in the F702W-band. This subsample has a threshold of F702W $\simeq 24$ (Vega magnitude; dashed line in Figure 4a), corresponding to $M_B \simeq -18$ at the mean redshift, $z = 0.61$.

In the infrared, the galaxy magnitudes are generally sensitive to the threshold $K_s \simeq 21$ (Vega magnitude), with the exception of the extensive campaign on the field 1622+268 (Steidel97) which is sensitive to $K_s \simeq 22$ (Vega magnitude; dashed lines in Figure 4b). For the high redshift subsample, $K_s \simeq 21$ corresponds $M_K \simeq -20$ at the mean redshift, $z = 0.61$. The majority of galaxies at low redshift were imaged in the r -band with SDSS. This subsample has a threshold of $r \simeq 22$ (AB magnitude; dotted line in Figure 4b), which, when converted to M_K using the conversion between $B-R$ and $B-K$, is roughly equal to $K_s \simeq 21$.

B -band luminosities have a range of $0.02 \leq L_B/L_B^* \leq 5.87$, with median $L_B/L_B^* = 0.611$. L_B/L_B^* as a function of z_{gal} is presented in Figure 4c. Point colors represent $W_r(2796)$, with open points indicating upper limits on $W_r(2796)$. Histograms show the distributions of B -band luminosity and galaxy redshift.

Luminosities in the K -band range from $0.006 \leq L_K/L_K^* \leq 9.71$ and have a median of $L_K/L_K^* = 0.493$. K -band luminosity as a function of z_{gal} is presented in Figure 4d with point colors indicating $W_r(2796)$ and upper limits on $W_r(2796)$ as open points. The distributions of L_K/L_K^* and z_{gal} are presented in histograms along their respective axes.

Galaxy rest-frame $B-K$ colors have a range of $0.04 \leq B-K \leq 4.09$, with median $B-K = 1.48$. $B-K$ as a function of z_{gal} is shown in Figure 5 and point colors represent $W_r(2796)$ strength, with open points indicating upper limits on $W_r(2796)$. Color and redshift distributions are shown in histograms. The mean and standard deviations in $B-K$ for three equal-sized redshift bins ($z < 0.403$, $0.403 \leq z < 0.709$, and $z \geq 0.709$) are plotted as black error bars. Horizontal error bars indicate the range in redshift for each bin. The horizontal dashed lines indicate the rest-frame $B-K$ color for each SED, where all three redshift bins are consistent with an Sbc

galaxy. This is in agreement with SDP94 and Zibetti et al. (2007), who find that galaxies with Mg II absorption have, on average, an Sbc SED type. The most common galaxy color is slightly redder than an Scd SED type.

Table 3 presents calculated galaxy and absorption properties for galaxies in MAGIIICAT. The listed columns are the (1) QSO identifier, (2) Julian 2000 designation (J-Name), (3) galaxy spectroscopic redshift, z_{gal} , (4) Mg II absorption redshift, z_{abs} , (5) Mg II equivalent width, $W_r(2796)$, (6) Mg II doublet ratio, (7) reference for columns 4, 5, and 6, (8) quasar-galaxy impact parameter, D , (9) K -correction to obtain M_B , (10) absolute B -band magnitude, M_B , (11) B -band luminosity, L_B/L_B^* , (12) K -correction to obtain M_K , (13) absolute K -band magnitude, M_K , (14) K -band luminosity, L_K/L_K^* , and (15) rest-frame color, $B-K$.

A summary of the absorption and galaxy properties of MAGIIICAT is presented in Table 4. We list the minimum, maximum, mean, and median values for each property.

4.1. Luminosity Functions

Prior to measurements of galaxy luminosity functions, $\Phi(M)$, out to $z = 1$ (e.g., Lilly et al. 1995; Lin et al. 1999; Fried et al. 2001; Wolf et al. 2003; Faber et al. 2007; Cirasuolo et al. 2010), selecting galaxies by Mg II absorption provided a compelling technique for compiling a presumably complete sample of intermediate redshift galaxies SDP94. Using absorption selection, SDP94 presented the B - and K -band luminosity functions of intermediate redshift galaxies associated with $W_r(2796) \geq 0.3 \text{ \AA}$.

In order to compare to and expand upon the work of SDP94, we measured the B - and K -band luminosity functions for MAGIIICAT galaxies. We divided the galaxies at all redshifts into two subsamples bifurcated by $W_r(2796) = 0.3 \text{ \AA}$. We also divided the galaxies into four subsamples bifurcated by $W_r(2796) = 0.3 \text{ \AA}$ and $z = 0.359$ (the median redshift). The average redshift is $z = 0.23$ for the low redshift subsample and $z = 0.61$ for the high redshift subsample. These averages translate to a 3.2 Gyr time spread.

Since the majority of the galaxies are absorption selected, we followed SDP94 and applied a gas cross section correction, $\langle R_{\text{gas}} \rangle^{-2}$, to the number of galaxies in each luminosity bin, where $\langle R_{\text{gas}} \rangle \propto \langle L/L^* \rangle^\beta$, where $\langle L/L^* \rangle$ is the mean luminosity of the bin and where β gives the empirically determined luminosity dependence. For the MAGIIICAT galaxies, we determined $\beta = 0.38$ for the B -band, and $\beta = 0.27$ for the K -band, as described in Paper II (Nielsen, Churchill, & Kacprzak 2012). The correction factor rectifies the relative volume probed by absorption line surveys at fixed luminosity under the assumption of completeness.

In Figures 6 and 7, we present the B - and K -band luminosity functions for MAGIIICAT galaxies. For reference, we have overplotted empirically determined Schechter luminosity functions from deep galaxy surveys (plus a single additive constant to roughly match the data at M_*). We show the $z = 0.3$ (solid curve) and $z = 1.1$ (dashed curve) luminosity functions from Faber et al. (2007) for the B -band using their “all galaxy sample” and Cirasuolo et al. (2010) for the K -band of galaxies in the UKIDSS UDF field. These curves roughly bracket the low and high redshift subsamples. For the B -band, the appropriate characteristic luminosities are $M_B^* = -21.1$ for $z = 0.3$ and $M_B^* = -21.5$ for $z = 1.1$. For the K -band, the appropriate characteristic luminosities are $M_K^* = -22.7$ for $z = 0.3$ and

$M_K^* = -23.1$ for $z = 1.1$.

For each binned data point, we computed the mean $B-K$ rest-frame color of the galaxies contributing to the bin and then color coded the point based upon the closest matching SED type (see Figure 5). Red data points indicate an average SED type for an elliptical (E) galaxy, yellow indicates Sbc on average, green indicates Scd on average, and blue indicates Magellanic-type irregular (Im) on average.

If we adopt the view that the galaxy surveys are magnitude-limited, we estimate that the completeness of MAGIIICAT begins to decline for $M_B > -18$ and $M_K > -17.5$ for the low redshift subsample and $M_B > -19$ and $M_K > -20$ for the high redshift subsample (see Figures 4a and 4b). We conservatively plotted the data in these luminosity bins as open points.

4.1.1. $W_r(2796)$ and Redshift Differences

For all MAGIIICAT galaxies with “weak” absorption or non-detections [$W_r(2796) < 0.3 \text{ \AA}$]⁸ (Figures 6a and 7a), the luminosity functions are more or less consistent with those of Faber et al. (2007) and Cirasuolo et al. (2010), though there is a trend for a flattening of the faint-end slopes, especially in $\Phi(M_B)$. The faint-end slopes of the “strong” absorbing galaxies [$W_r(2796) \geq 0.3 \text{ \AA}$] (Figures 6b and 7b), are less certain, but suggestive of a flattening of the faint-end slope relative to the Faber et al. (2007) and Cirasuolo et al. (2010) luminosity functions.

For the subsamples over the full redshift interval, we find no statistical differences between the $\Phi(M_B)$ for weak and strong absorbers (panel a vs. b of Figure 6) as deduced from a KS test on the unbinned luminosities. The same result applies for $\Phi(M_K)$ for weak and strong absorbers (panel a vs. b of Figure 7). Similarly, there are no statistical differences between the $\Phi(M_B)$ of weak and strong absorbing galaxies in the low redshift subsample (panel c vs. d of Figure 6) nor in the $\Phi(M_B)$ in the high redshift subsample (panel e vs. f of Figure 6). The same result holds for the $\Phi(M_K)$ of weak and strong absorbing galaxies for both the low and high redshift subsamples.

For each band, we examined for redshift evolution for the subsample with weak absorption or non-detections (panels c vs. e of Figures 6 and 7) and for the subsample with strong absorption (panels d vs. f of Figures 6 and 7). For $\Phi(M_B)$ of the weak absorbing galaxies, we find redshift evolution at a 3.4σ significance level in the sense that the luminosity function at low redshift is shifted ~ 0.5 magnitudes dimmer relative to high redshift for galaxies with $M_B < -18$. We find only a suggestive trend for redshift evolution of $\Phi(M_B)$ of the strong absorbing galaxies (2.4σ). There is also a possible trend for redshift evolution in the K -band of the strong absorbing galaxies (2.4σ), but no evidence for the weak absorbing galaxies.

For the B -band luminosities, we note that the observed trends from lower to higher redshift (i.e., flattening of the faint-end slope and relative overabundance at higher luminosity) are reminiscent of the Malmquist bias that plagues magnitude-limited surveys. Given the heterogeneous selection methods used by the various works from which we constructed MAGIIICAT, it is difficult to quantify the degree to which this may be an issue.

⁸ By examining gas defined by $W_r(2796) < 0.3 \text{ \AA}$, whether Mg II absorption is detected or not detected to the sensitivities afforded by the data, we are probing a well-defined gas regime, i.e., gas that does not give rise to Mg II absorption with $W_r(2796) \geq 0.3 \text{ \AA}$. The only assumption is that there is gas probed by the quasar line of sight within the region we would consider to be the CGM.

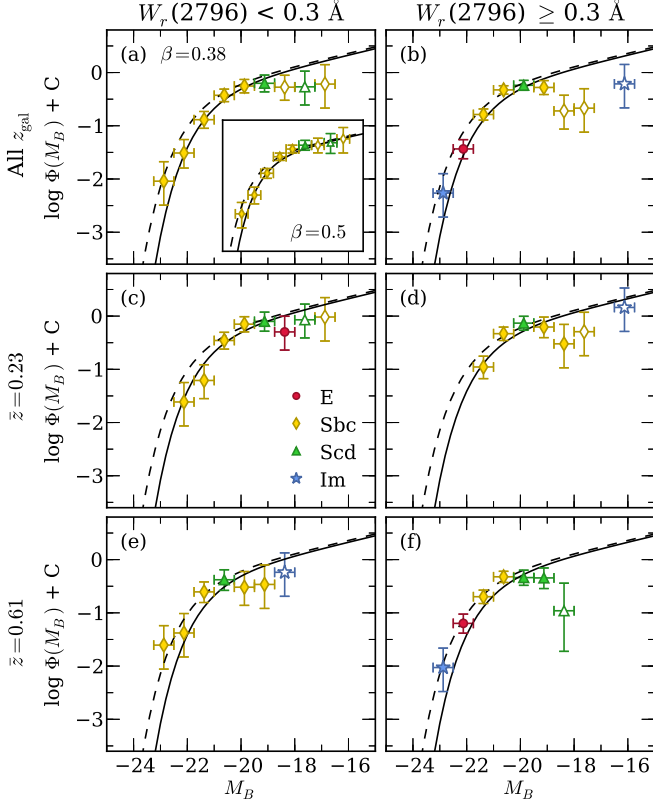


FIG. 6.— B -band luminosity functions for $W_r(2796) < 0.3 \text{ \AA}$ (a, c, and e) and $W_r(2796) \geq 0.3 \text{ \AA}$ (b, d, and f). Galaxies at all redshifts are included in panels a and b, while galaxies with $z < \langle z \rangle$ are in panels c and d (mean $z = 0.22$), and galaxies with $z \geq \langle z \rangle$ are in panels e and f (mean $z = 0.61$), where $\langle z \rangle = 0.359$. The solid and dashed curves are $z = 0.3, 1.1$ Schechter functions, respectively, from Faber et al. (2007). Data point colors and types are assigned according to the mean color of the galaxies in the bin. Red circles indicate the mean color in the bin is closest to an elliptical (E) SED type, yellow diamonds indicate Sbc, green triangles indicate Scd, and blue stars indicate a Magellanic-type irregular (Im) SED type. Open points are where the completeness of the sample declines. The inset of panel (a) illustrates how the observed luminosity function changes with the gas cross section correction $\langle R_{\text{gas}} \rangle^{-2} \propto \langle L/L_B^* \rangle^{-2\beta}$.

4.1.2. Color Sequence Along $\Phi(M_B)$ and $\Phi(M_K)$

The MAGIIICAT galaxies (full catalog) exhibit a significant correlation between $B-K$ and M_K (7.8σ), but only a weak trend between $B-K$ and M_B (2.0σ). For the subsample of strong absorbing galaxies (Figure 7b) the correlation between $B-K$ and M_K is significant to 6.6σ and for the weak absorbing galaxy subsample (Figure 7a) the correlation is 3.6σ . The weak trend between $B-K$ and M_B is dominated by strong absorbing galaxies (2.0σ , Figure 6f).

The weakest trends (less than 3σ) between $B-K$ and M_K are found for the strong absorbing galaxies at low redshift (Figure 7d) and the weak absorbing galaxies at high redshift (Figure 7e), even though the mean colors suggest a strong trend. $B-K$ and M_K are correlated at the 3.2σ level for weak absorbing galaxies at low redshift (Figure 7c) and 6.4σ for strong absorbing galaxies at high redshift (Figure 7f). There is no correlation between $B-K$ color and M_B for any of the subsamples presented in Figures 6 except for Figure 6f, where there is a 3.0σ correlation.

The trends and strong correlations between $B-K$ and M_K are reflected in the color sequence of the data points for $\Phi(M_K)$ in Figure 7; the higher the infrared luminosity, the red-

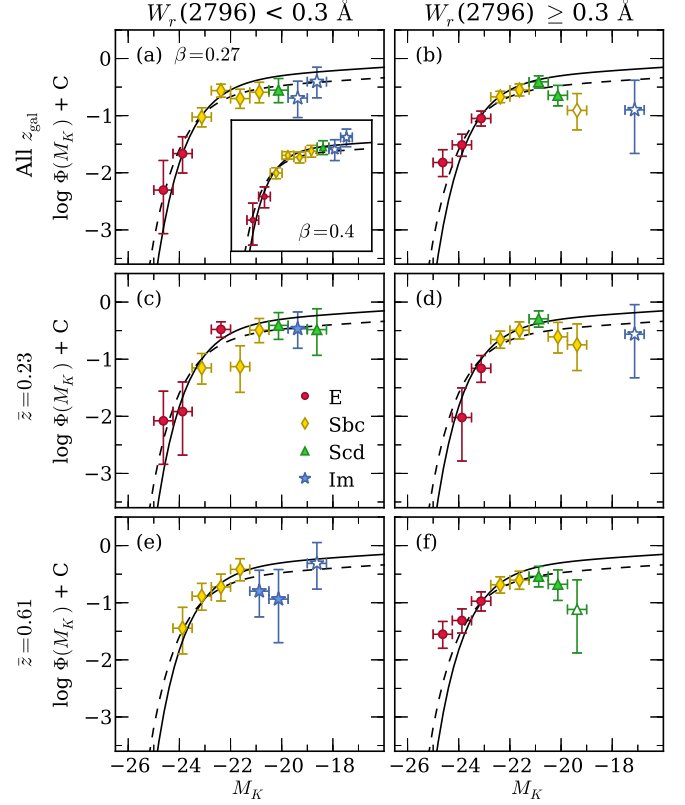


FIG. 7.— K -band luminosity functions for $W_r(2796) < 0.3 \text{ \AA}$ (a, c, and e) and $W_r(2796) \geq 0.3 \text{ \AA}$ (b, d, and f). Galaxies at all redshifts are included in panels a and b, while galaxies with $z < \langle z \rangle$ are in panels c and d (mean $z = 0.22$), and galaxies with $z \geq \langle z \rangle$ are in panels e and f (mean $z = 0.61$), where $\langle z \rangle = 0.359$. The solid and dashed curves are $z = 0.3, 1.1$ Schechter functions, respectively, from Cirasuolo et al. (2010). Point types and colors are the same as described in Figure 6. The inset of panel (a) illustrates how the observed luminosity function changes with the gas cross section correction $\langle R_{\text{gas}} \rangle^{-2} \propto \langle L/L_K^* \rangle^{-2\beta}$.

der the mean galaxy color. Interestingly, for both the B -band and the K -band, KS tests reveal no significant differences in the distribution of $B-K$ between the weak and strong absorbing galaxies at low redshift, at high redshift, nor for all redshifts.

Though the overall color distribution may not differ between the galaxy subsamples, the average SED of the bright end of the K -band luminosity function corresponds to early-type E galaxies and the faint end corresponds to late-type galaxies (Sbc, Scd, and Im). On the contrary, there is no clear color differential along the luminosity sequence of $\Phi(M_B)$. The average color in virtually all B -band luminosity bins is that of an Sbc or Scd SED.

4.1.3. The $W_r(2796) \geq 0.3 \text{ \AA}$ High-Redshift Subsample

The strong absorbing [$W_r(2796) \geq 0.3 \text{ \AA}$] high redshift subsamples (Figures 6f and 7f) are most appropriately compared to the SDP94 luminosity functions, which correspond to $\langle z \rangle = 0.65$.

SDP94 find that $\Phi(M_B)$ for Mg II absorption selected galaxies turns down (or “rolls off”) relative to the faint-end slope of $\Phi(M_B)$ for field galaxies starting roughly at 1.5 magnitudes below M_B^* , whereas $\Phi(M_K)$ for Mg II absorption selected galaxies is consistent with $\Phi(M_K)$ of field galaxies to roughly 3.1 magnitudes below M_K^* (i.e., $L_K/L_K^* \simeq 0.05$). They infer that the absorption selected galaxies “missing” from the faint

end of $\Phi(M_B)$ are Sd types and later.

SDP94 also report a strong correlation between $B-K$ and M_K in that fainter galaxies in the K -band are bluer, and also find no such correlation between $B-K$ and M_B . Incorporating the correlation between $B-K$ and M_K , they argue that faint blue galaxies (e.g., Ellis 1997) do not typically exhibit Mg II absorption with $W_r(2796) \geq 0.3 \text{ \AA}$ and that this explains the difference in the behavior of the faint-end slopes of $\Phi(M_B)$ and $\Phi(M_K)$. They further conclude that the gas cross section is more likely to be governed by galaxy mass ($\propto L_K$) than by star formation. We note that this latter statement is inconsistent with our finding that the covering fraction of Mg II absorption is invariant with galaxy halo mass for multiple $W_r(2796)$ thresholds (Churchill et al. 2013b).

For MAGIICAT galaxies, the measured $\Phi(M_B)$ for strong absorbing galaxies at high redshift (Figure 6f) is suggestive of a faint-end roll off around 1.5 magnitudes below M_B^* , consistent with the SDP94 result. Similarly, we find a possible faint-end roll off in $\Phi(M_K)$ for the strong absorbing galaxies at high redshift (Figure 7f) starting at roughly 2 magnitudes below M_K^* . This latter result is contrary to the findings of SDP94. Note that, for this subsample of the MAGIICAT galaxies, the data extend roughly an additional magnitude below M_K^* as compared to the SDP94 sample.

4.1.4. Interpreting $\Phi(M_B)$ and $\Phi(M_K)$

Interpreting and comparing the functional forms of $\Phi(M_B)$ and $\Phi(M_K)$ is rendered difficult due to the heterogeneous selection methods of the galaxies in MAGIICAT. The majority of galaxies are “absorption selected”, whereas some galaxies are magnitude-limited or volume-limited selected. We have applied “gas cross section” corrections to all galaxies in the sample, which is a correct procedure for absorption selected galaxies.

In the cases where galaxies are searched for and identified based upon prior knowledge of a Mg II absorption redshift, there can be ambiguity as to whether the galaxy is the only galaxy connected to the Mg II absorption. It is always possible that an additional galaxy is in close projection with the background quasar; given the clustering properties of galaxies, this would be more rare for two galaxies at the bright end of the luminosity function, but it could be more probable as fainter galaxies are considered. These can be found only with careful point spread function subtraction of the quasar, which has been performed for all of the quasar fields surveyed from the ground by GB97 and for the majority of the fields originally surveyed by SDP94 (in both ground-based and *HST* images, where the latter was performed by A. Shapley, private communication, unpublished). However, such analysis has not been performed for the remainder of the galaxies in MAGIICAT. Furthermore, the absorption selection approach usually entails an incomplete survey of the galaxies in the quasar field. If an additional galaxy (or galaxies) might be discovered in a given quasar field to have a redshift consistent with the Mg II absorption, the galaxies would reclassify as a “group” and would not be included in the present work.

In the cases where galaxies are identified in apparent magnitude- or volume-limited surveys, the point spread function issue is just as relevant. Furthermore, apparent magnitude-limited surveys would suffer from faint-end incompleteness and/or Malmquist bias.

Though the shapes of the luminosity functions presented in Figures 6 and 7 are suggestive of a relative paucity of sub- L^* galaxies as compared to field galaxies, or perhaps even

a roll over in the faint-end slopes, the above considerations make it difficult to assess whether selection effects are at play. Though the gas cross section corrections we applied act to reduce the value of $\Phi(M)$ for $L > L^*$ galaxies, the corrections *increase* the value of $\Phi(M)$ for sub- L^* galaxies; the correction factor increases with decreasing luminosity. Thus, discrepancies between the observed luminosity functions and a Schechter function could result from our not applying the proper cross section correction.

As an exercise, we could attempt to recover the Schechter function (under the assumption that the luminosity function of *all* galaxies follows this functional form) by varying the β in the gas cross section correction $\langle R_{\text{gas}} \rangle^{-2} \propto \langle L/L^* \rangle^{-2\beta}$. In essence, we then learn something about the gas cross sections of galaxies as a function of luminosity. In the insets of Figures 6a and 7a, we provide examples of a $\simeq 0.1$ increase in β for the $W_r(2796) < 0.3 \text{ \AA}$ subsamples over all redshifts. This illustrates that if we have a steeper luminosity dependence on the gas cross section, especially at the faint end, the data can be better matched to a Schechter function. That is, matching the observed luminosity function of absorption selected galaxies to the Schechter function can, in principle, be used to constrain the luminosity dependence of the gas cross section. Most importantly, with an increased sample size (larger than MAGIICAT), we might be able to determine that the gas cross section does not follow a constant power law, that the slope β is also luminosity dependent. For example, it is possible to have all subsamples conform to a Schechter function if we parameterize β to have luminosity dependence such that the gas cross section of low luminosity galaxies declines more rapidly with decreasing luminosity than it does for high luminosity galaxies.

Even using the presented luminosity functions, we can still infer that, in general, galaxy $B-K$ color is independent of galaxy B -band luminosity. Regardless of the B -band luminosity, the *average* color is consistent with that of an Sbc/Scd galaxy. However, there is a $B-K$ color sequence in that the greater the infrared luminosity, the redder the $B-K$ color. This is a highly significant result. If M_K serves as a very crude proxy for *stellar* mass, the luminosity functions suggest that galaxies with lower stellar masses with detectable Mg II absorbing gas comprise bluer (younger) stellar populations.

This might suggest that a detectable Mg II absorbing CGM may not be present in low stellar mass red galaxies; only the lower stellar mass galaxies with bluer (younger) stellar populations give rise to detectable Mg II absorption. Since the roll over at the faint-end is more pronounced for galaxies with $W_r(2796) \geq 0.3 \text{ \AA}$ absorbing gas, we might infer that weaker Mg II absorption is preferentially found in the lower stellar mass galaxies.

5. SUMMARY AND CONCLUSIONS

We compiled, from our own work and the literature, the Mg II Absorbing-Galaxy Catalog, MAGIICAT, consisting of galaxies with intermediate redshifts to study the galaxy-circumgalactic medium interaction as probed by Mg II $\lambda\lambda 2796, 2803$ absorption. The catalog presented here contains 182 isolated galaxies with spectroscopic redshifts $0.07 \leq z \leq 1.1$, impact parameters $D < 200 \text{ kpc}$ from a background quasar, and known Mg II absorption or a 3σ upper limit on absorption less than or equal to 0.3 \AA . A summary of the minimum, maximum, mean, and median values for absorption and galaxy properties in MAGIICAT is presented in

Table 4.

All values that depend on cosmological parameters have been recalculated, including quasar-galaxy impact parameters, absolute magnitudes, and luminosities. This standardizes the galaxy properties and allows for a comparison of galaxies whose properties were placed on different cosmologies over the last ~ 20 years. Absolute magnitudes and luminosities were calculated in the B -band for all galaxies and in the K -band for all but 18. We find that the average rest-frame $B-K$ color of MAGIIICAT galaxies is consistent with an Sbc galaxy, though the most common galaxy color is slightly redder than an Scd galaxy. The average color agrees with SDP94 and Zibetti et al. (2007).

We present the B - and K -band luminosity functions, $\Phi(M)$, for subsamples split by $W_r(2796) < 0.3 \text{ \AA}$ (“weak”) and $W_r(2796) \geq 0.3 \text{ \AA}$ (“strong”), and by low redshift and high redshift, cut by $z = 0.359$. We find that the luminosity functions in both bands for galaxies with weak absorption or non-detections are more-or-less consistent with Faber et al. (2007) and Cirasuolo et al. (2010), while the strong absorbing galaxies may be flatter in the faint-end slope. Comparing the strong, high redshift subsample to SDP94, we find the suggestive faint-end roll off of the luminosity function in the B -band consistent, while the possible roll off in the K -band is contrary. No statistical difference between weak and strong subsamples for all, low redshift, and high redshift galaxies is present in either the B - or the K -band. The B -band may show redshift evolution in both the weak and strong subsamples, but in the K -band, evolution may only be present in the strong subsample. These above statements depend upon the gas cross section correction factor that we have applied to the data. We discussed how the luminosity functions can, in principle, be used to constrain the dependence of the gas cross section on galaxy luminosity.

We find a correlation between $B-K$ and M_K for the full sample (7.8σ), but only a weak correlation between $B-K$ and M_B (2.0σ), consistent with the findings of SDP94. Splitting MAGIIICAT into weak absorbers, strong absorbers, low redshift, and high redshift subsamples, we find the correlations in both bands are dominated by the high redshift, strong absorbing galaxies. As M_K becomes brighter, the mean galaxy color becomes redder. On the other hand, the mean color of most magnitude bins in the B -band luminosity functions is consistent with an Sbc/Scd SED.

The behavior of the luminosity functions suggest that only the lower stellar mass galaxies with bluer (younger) stellar populations give rise to detectable Mg II absorption. Comparing the faint-end roll over between galaxies with $W_r(2796) \geq 0.3 \text{ \AA}$ and $W_r(2796) < 0.3 \text{ \AA}$ absorbing gas, it would seem that in lower stellar mass galaxies, weaker Mg II absorption would be observed more commonly.

Further analysis has already been conducted with all or a portion of the galaxies in MAGIIICAT. Kacprzak, Churchill, & Nielsen (2012) studied the effect of galaxy orientation on Mg II absorption. They found that Mg II gas is preferentially found along the galaxy major and minor axes, where the covering fraction of Mg II absorption as a function of orientation is enhanced by as much as 20%–30% along the major and minor axes. This bimodality was found to be driven by blue galaxies and may indicate outflowing gas with an opening angle of 100° and inflowing gas with an opening angle of 40° .

Using halo abundance matching, Churchill et al. (2013b,c)

obtained the galaxy virial masses for all galaxies in MAGIIICAT and studied the $W_r(2796)$ - D anti-correlation and Mg II covering fractions, both as a function of galaxy virial mass. They found that the Mg II CGM has projected absorption profile that follows $(D/R_{\text{vir}})^{-2}$, where R_{vir} is the virial radius, indicating a self-similar behavior with virial mass. They also find that $W_r(2796)$ increases with virial mass in finite ranges of D but is constant in finite ranges of D/R_{vir} , and that covering fractions are unchanged as a function of galaxy virial mass within a given D or D/R_{vir} . Their results are contrary to the theoretical prediction that cold-mode accretion is shut down in high-mass galaxies (Birnboim & Dekel 2003; Dekel & Birnboim 2006; Stewart et al. 2011).

Nielsen, Churchill, & Kacprzak (2012) [Paper II of this series] presented an analysis of how $W_r(2796)$, covering fractions, and the radial extent of the Mg II CGM depend on impact parameter, galaxy redshift, B - and K -band luminosities, and $B-K$ color. They found that the anti-correlation between $W_r(2796)$ and D can be characterized by a log-linear fit which levels off at low D . The scatter on the $W_r(2796)$ - D plane may be due to galaxy luminosity, where more luminous galaxies have larger $W_r(2796)$ at a fixed D . They also found that the covering fraction decreases with increasing D and increasing $W_r(2796)$ threshold. More luminous, bluer, and higher redshift galaxies have larger covering fractions than less luminous, redder, and lower redshift galaxies at a given D . The luminosity-scaled radial extent of the Mg II CGM is more sensitive to luminosity in the B -band than in the K -band. The radial extent has a steeper luminosity dependence for red galaxies than blue galaxies, and for low redshift than high redshift galaxies.

In future work we intend to apply multivariate analysis methods to MAGIIICAT, incorporating the galaxy virial mass estimates of the galaxies from Churchill et al. (2013c) as well as Mg II kinematics and the low- and high-ionization absorption strengths of the CGM. We also plan to utilize the sample of group galaxies we obtained with the present work, comparing the group galaxies to the isolated galaxies. Mining the *Hubble Space Telescope* archive for H I and UV low- and high-ionization metal-line transitions will be useful for developing a more complete understanding of the CGM properties of MAGIIICAT galaxies.

We thank the referee for helpful comments which improved the manuscript. We also thank Jacqueline Bergeron for providing details on the observations conducted in Guillemin & Bergeron (1997), Chuck Steidel for communicating detailed aspects relating to the work by Steidel, Dickinson, & Persson (1994), including access to unpublished materials, and David Law for additional magnitudes. We extend our gratitude to all the researchers whose hard work over the last two decades resulted in the growing database of published galaxies in quasar fields. Without their efforts, this work would not have been possible. This research was primarily supported through grant HST-AR-12646 provided by NASA via the Space Telescope Science Institute, which is operated by the Association of Universities for Research in Astronomy (AURA) under NASA contract NAS 5-26555. This work was also supported by the Research Enhancement Program provided by NASA’s New Mexico Space Grant Consortium (NMSGC). N.M.N. was also partially supported through a NMSGC Graduate Fellowship and a Graduate Research Enhancement Grant (GREG)

sponsored by the Office of the Vice President for Research at New Mexico State University. M.T.M. thanks the Australian Research Council for a QEII Research Fellowship (DP0877998) and Discovery Project grant (DP130100568). This research has made extensive use of the SAO/NASA Astrophysics Database System (ADS), operated by the Smithsonian Astrophysical Observatory under contract with NASA, the NASA/IPAC Extragalactic Database (NED), operated by

the Jet Propulsion Laboratory and California Institute of Technology, under contract with NASA, and the SIMBAD database, operated at Centre de Données, Strasbourg, France. This research has also made use of the Spanish Virtual Observatory (<http://svo.cab.inta-csic.es>) supported from the Spanish MICINN / MINECO through grants AyA2008-02156, AyA2011-24052

APPENDIX

A. K -CORRECTIONS

For a galaxy at redshift z and observed in bandpass y , the K -correction between bandpass y and desired bandpass x is:

$$K_{xy} = 2.5 \log(1+z) + 2.5 \log \left[\frac{\int R_x(\lambda) \lambda f_\lambda(\lambda) d\lambda}{\int R_y(\lambda) \lambda f_\lambda(\lambda/[1+z]) d\lambda} \right] + 2.5 \log \left[\frac{\int R_y(\lambda) \lambda f_\lambda^s(\lambda) d\lambda}{\int R_x(\lambda) \lambda f_\lambda^s(\lambda) d\lambda} \right], \quad (\text{A1})$$

where $R_y(\lambda)$ is the response curve of the y -band, $R_x(\lambda)$ is the response of the x -band, $f_\lambda(\lambda)$ is the flux density of the object being observed in the object's rest frame, $f_\lambda(\lambda/[1+z])$ is the flux density of the redshifted object in the observer frame, and $f_\lambda^s(\lambda)$ is the standard Vega or AB spectrum. The first two terms of the K -correction correct for the fact that the observed object's spectrum is stretched and shifted redwards at larger z . The last term is the color term which corrects for different observed (y) and desired (x) bandpasses. If these bandpasses are identical, the color term cancels out.

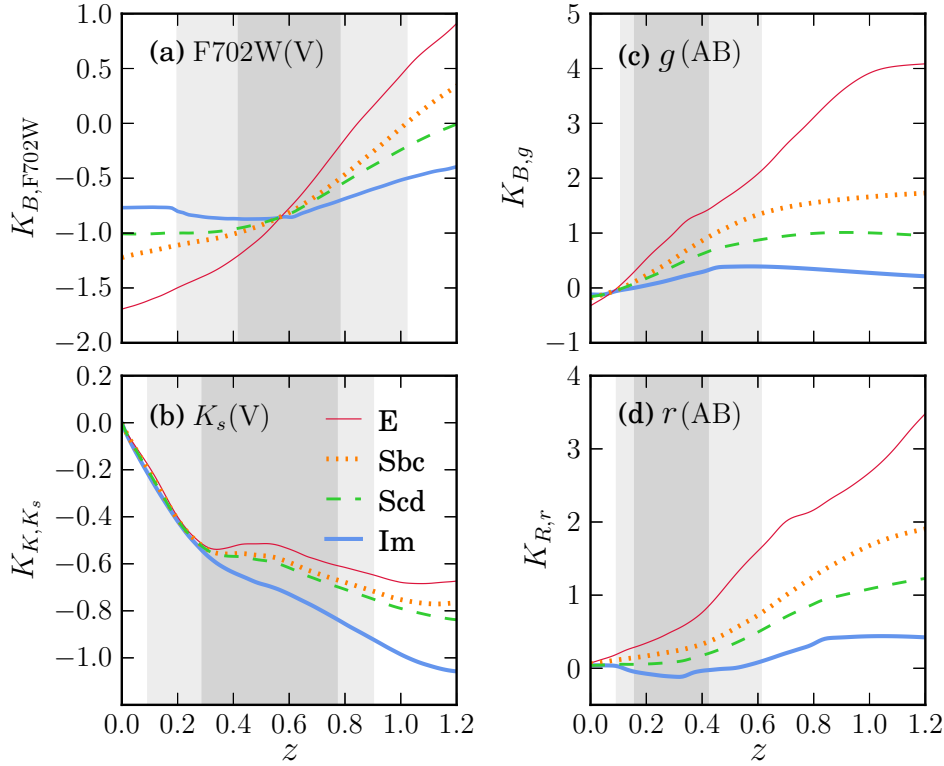


FIG. A1.— The K -corrections between various bands as a function of redshift for spectral energy distributions E, Sbc, Scd, and Im. Apparent magnitudes in the F702W(Vega) and g (AB) bands were K -corrected to the B -band, K_s (Vega) to the K -band, and r (AB) to the R -band. The lighter gray shading indicates the full redshift region over which the K -corrections were applied while the darker gray shading indicates where the central 68% of the galaxies reside.

We obtained the required filter response curves, $R_x(\lambda)$ and $R_y(\lambda)$, from the website associated with the facility used to observe a given galaxy, or from the author of the work. Chuck Steidel (private communication) kindly provided us both the R_s and the K_s response curves while Jacqueline Bergeron (private communication) provided the R_{EFOSC} response curve. We also used the Spanish Virtual Observatory Filter Profile Service⁹. We retrieved the Vega composite flux standard spectrum “alpha_lyr_stis_005” from the STScI Calibration Database System, Calspec¹⁰. For AB magnitudes, we calculated a standard AB spectrum, defined as a hypothetical source with $F_\nu^{(\text{AB})} = 3.63 \times 10^{-20} \text{ [erg s}^{-1} \text{ cm}^{-2} \text{ Hz}^{-1}]$.

⁹ <http://svo2.cab.inta-csic.es/theory/fps/>

¹⁰ <http://www.stsci.edu/hst/observatory/cdbs/calspec.html>

Figure A1 presents the K -correction for each SED as a function of redshift for Vega magnitudes F702W and K_s , and AB magnitudes g and r , the four most common bandpasses in MAGIIICAT. Vega magnitudes F702W and K_s were corrected to Vega magnitudes B and K , respectively, while AB magnitudes g and r were corrected to AB magnitudes B and R , respectively. The lighter gray shading indicates the full galaxy redshift range over which the K -corrections were applied for that band. The darker gray shading indicates where the central 68% of the galaxies reside.

We determined the constants of conversion between Vega and AB magnitudes by calculating the B - and K -band absolute magnitudes for a given SED alternately using the Vega spectrum and the AB spectrum. Taking the difference of the Vega and AB magnitudes in each band produced the conversions $B(AB) = B(V) - 0.0873$ and $K(AB) = K(V) + 1.8266$. These constants are comparable to the values -0.09 (B -band) and 1.85 (K -band) which are presented in Table 1 of Blanton & Roweis (2007). We applied these constants to the K -corrected apparent magnitudes when necessary.

B. SELECTING SPECTRAL ENERGY DISTRIBUTIONS FOR K -CORRECTIONS

For $f_\lambda(\lambda)$ in Equation A1, we did not have direct access to the galaxy spectra for MAGIIICAT galaxies. Therefore we rely on Coleman et al. (1980) spectral energy distribution (SED) templates which were extended to shorter and longer wavelengths by Bolzonella et al. (2000) using synthetic spectra created with the GISSEL98 code (Bruzual & Charlot 1993). These SEDs were distributed with and used by the HYPERZ¹¹ photometric redshift code (Bolzonella et al. 2000).

To select which K -correction to apply, we determined which SED each galaxy in MAGIIICAT most closely resembles. We compared the observed colors of the galaxy to each SED type at the galaxy's redshift. In cases where the observed galaxy color was in between the color of two different SEDs, the closest SED was selected. Where no observed colors were available due to a lack of a second band, the galaxy was classified as an Sbc galaxy, the average type for MgII absorbing galaxies (SDP94; Zibetti et al. 2007).

We calculated the SED observed colors by first determining the rest-frame colors of each SED. This was done by calculating the appropriate apparent magnitudes of the SEDs at $z = 0$ and taking the difference of the magnitudes, making sure to use the correct filter and AB/Vega combinations. We then calculated the necessary K -corrections at redshifts $0 < z < 1.2$ with the methods described in Appendix A. To obtain the observed SED colors for the redshift range of MAGIIICAT, we combined these K -corrections with the rest-frame SED colors, e.g., $(F702W - K_s)_{z>0} = (F702W - K_s)_{z=0} + [K_{K_s}(z) - K_{F702W}(z)]$, where the terms in the square brackets are the K -corrections for the K_s and F702W bands, respectively, for $z > 0$.

The two most common observed colors in the sample are $F702W - K_s$ (Vega), and $g - r$ (AB). These colors are presented in Figure B1 for all SEDs. The rest of the observed colors follow the trend of $F702W - K_s$ due to a combination of a red band with an infrared band. Our $g - r$ colors are consistent with Hewett et al. (2006), who present $g - r$ for the extended Coleman SEDs.

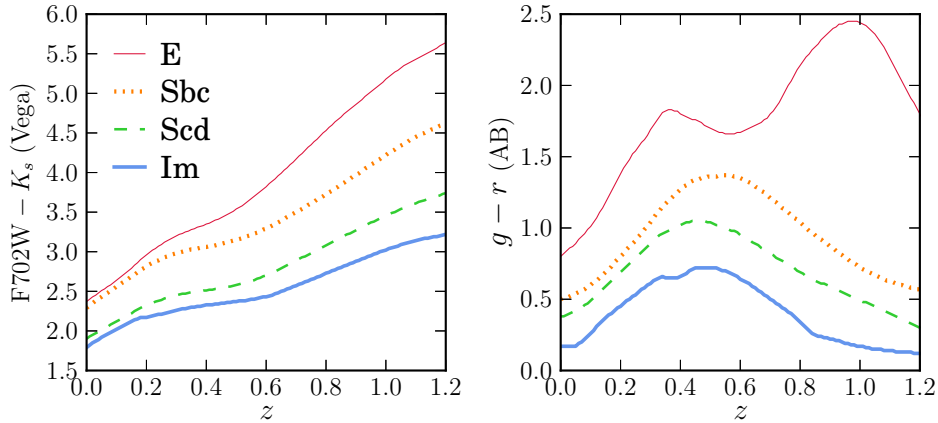


FIG. B1.— Observed colors, $F702W - K_s$ (Vega) and $g - r$ (AB), for the galaxy SEDs as a function of redshift. These two colors are the most common observed colors in MAGIIICAT. The rest of the colors follow the same trend as $F702W - K_s$.

C. $B - R$ TO $B - K$ REST-FRAME COLOR CONVERSION

For SDSS galaxies which did not have a K -band magnitude available, we determined M_K indirectly by using a conversion between rest-frame colors $B - R$ and $B - K$. We calculated the rest-frame $B - K$ and $B - R$ colors for each SED using the methods applied in Appendix B. The points in Figure C1 present the rest-frame colors for each SED. The SED colors appear to follow a linear trend so a linear least-squares fit was performed. The fit has the form $(B - K) = 1.86(B - R) + 0.02$ and is presented as the solid line in Figure C1. We therefore obtained absolute K -band magnitudes, M_K , for each SDSS galaxy by applying the equation $M_K = M_B - (B - K) = M_B - 1.86(B - R) - 0.02$.

REFERENCES

- Barton, E. J., & Cooke, J. 2009, AJ, 138, 1817 (BC09)
 Bergeron, J., & Boiss , P. 1991, A&A, 243, 334
 Bergeron, J., Petitjean, P., Sargent, W. L. W., et al. 1994, ApJ, 436, 33

¹¹ <http://webast.ast.obs-mip.fr/hyperz/>

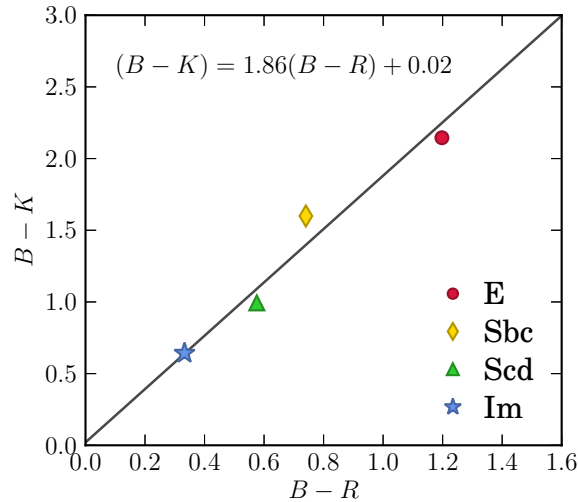


FIG. C1.— The relationship between rest-frame colors $B-K$ and $B-R$ for the SEDs. Point types and colors indicate the SED type. The data appear to follow the linear relation listed on the figure.

- Bergeron, J., & Stasińska, G. 1986, *A&A*, 169, 1
- Birnboim, Y., & Dekel, A. 2003, *MNRAS*, 345, 349
- Birnboim, Y., Dekel, A., & Neistein, E. 2007, *MNRAS*, 380, 339
- Blanton, M. R., & Roweis, S. 2007, *AJ*, 133, 734
- Bolzonella, M., Miralles, J.-M., & Pelló, R. 2000, *A&A*, 363, 476
- Bordoloi, R., Lilly, S. J., Knobel, C., et al. 2011, *ApJ*, 743, 10
- Bouché, N., Hohensee, W., Vargas, R., et al. 2012, *MNRAS*, 426, 801
- Bouché, N., Murphy, M. T., Péroux, C., Csabai, I., & Wild, V. 2006, *MNRAS*, 371, 495
- Bowen, D. V., & Chelouche, D. 2011, *ApJ*, 727, 47
- Brown, B. W., Hollander, M., & Korwar, R. M. 1974, in *Reliability and Biometry*, 327
- Bruzual A. G., & Charlot, S. 1993, *ApJ*, 405, 538
- Chelouche, D., & Bowen, D. V. 2010, *ApJ*, 722, 1821
- Chen, H.-W., Helsby, J. E., Gauthier, J.-R., Shectman, S. A., Thompson, I. B., & Tinker, J. L. 2010a, *ApJ*, 714, 1521 (Chen10)
- Chen, H.-W., Lanzetta, K. M., & Webb, J. K. 2001a, *ApJ*, 556, 158
- Chen, H.-W., Lanzetta, K. M., Webb, J. K., & Barcons, X. 1998, *ApJ*, 498, 77
- Chen, H.-W., Lanzetta, K. M., Webb, J. K., & Barcons, X. 2001b, *ApJ*, 559, 654
- Chen, H.-W., Wild, V., Tinker, J. L., et al. 2010b, *ApJ*, 724, L176
- Chen, H.-W., & Tinker, J. L. 2008, *ApJ*, 687, 745 (CT08)
- Churchill, C. W., Kacprzak, G. G., Nielsen, N. M., Steidel, C. C., Murphy, M. T. 2013a, *ApJ*, submitted (Churchill13)
- Churchill, C. W., Kacprzak, G. G., & Steidel, C. C. 2005, *IAU Colloq.* 199: Probing Galaxies through Quasar Absorption Lines, 24
- Churchill, C. W., Kacprzak, G. G., Steidel, C. C., & Evans, J. L. 2007, *ApJ*, 661, 714
- Churchill, C. W., Mellon, R. R., Charlton, J. C., Jannuzi, B. T., Kirhakos, S., Steidel, C. C., & Schneider, D. P. 2000a, *ApJS*, 130, 91
- Churchill, C. W., Nielsen, N. M., Kacprzak, G. G., & Trujillo-Gomez, S. 2013b, *ApJ*, 763, L42
- Churchill, C. W., Rigby, J. R., Charlton, J. C., & Vogt, S. S. 1999, *ApJS*, 120, 51
- Churchill, C. W., Steidel, C. C., & Vogt, S. S. 1996, *ApJ*, 471, 164
- Churchill, C. W., Trujillo-Gomez, S., Nielsen, N. M., & Kacprzak, G. G., 2013c, *ApJ*, submitted (Paper III)
- Cirasuolo, M., McLure, R. J., Dunlop, J. S., Almaini, O., Foucaud, S., & Simpson, C. 2010, *MNRAS*, 401, 1166
- Coil, A. L., Weiner, B. J., Holz, D. E., et al. 2011, *ApJ*, 743, 46
- Coleman, G. D., Wu, C.-C., & Weedman, D. W. 1980, *ApJS*, 43, 393
- Dekel, A., & Birnboim, Y. 2006, *MNRAS*, 368, 2
- Dekker, H., D'Odorico, S., Kaufer, A., Delabre, B., & Kotzlowski, H. 2000, *Proc. SPIE*, 4008, 534
- Ellis, R. S. 1997, *ARA&A*, 35, 389
- Evans, J. L. 2011, Ph.D. Thesis, New Mexico State University
- Faber, S. M., et al. 2007, *ApJ*, 665, 265
- Fried, J. W., von Kuhlmann, B., Meisenheimer, K., et al. 2001, *A&A*, 367, 788
- Gauthier, J.-R., & Chen, H.-W. 2011, *MNRAS*, 418, 2730 (GC11)
- Guillemin, P., & Bergeron, J. 1997, *A&A*, 328, 499 (GB97)
- Hewett, P. C., Warren, S. J., Leggett, S. K., & Hodgkin, S. T. 2006, *MNRAS*, 367, 454
- Kacprzak, G. G., Churchill, C. W., Barton, E. J., & Cooke, J. 2011a, *ApJ*, 733, 105 (KCBC11)
- Kacprzak, G. G., Churchill, C. W., Ceverino, D., et al. 2010, *ApJ*, 711, 533
- Kacprzak, G. G., Churchill, C. W., Evans, J. L., Murphy, M. T., & Steidel, C. C. 2011b, *MNRAS*, 416, 3118 (KCEMS11)
- Kacprzak, G. G., Churchill, C. W., & Nielsen, N. M. 2012, *ApJ*, 760, L7
- Kacprzak, G. G., Churchill, C. W., Steidel, C. C., & Murphy, M. T. 2008, *AJ*, 135, 922
- Kacprzak, G. G., Churchill, C. W., Steidel, C. C., Spitler, L. R., & Holtzman, J. A. 2012, *MNRAS*, 427, 3029
- Kacprzak, G. G., Murphy, M. T., & Churchill, C. W. 2010, *MNRAS*, 406, 445 (KMC10)
- Kereš, D., Katz, N., Fardal, M., Davé, R., & Weinberg, D. H. 2009, *MNRAS*, 395, 160
- Kereš, D., Katz, N., Weinberg, D. H., & Davé, R. 2005, *MNRAS*, 363, 2
- Kim, A., Goobar, A., & Perlmutter, S. 1996, *PASP*, 108, 190
- Lanzetta, K. M., & Bowen, D. 1990, *ApJ*, 357, 321
- Lanzetta, K. M., Bowen, D. V., Tytler, D., & Webb, J. K. 1995, *ApJ*, 442, 538
- Lilly, S. J., Tresse, L., Hammer, F., Crampton, D., & Le Fevre, O. 1995, *ApJ*, 455, 108
- Lin, H., Yee, H. K. C., Carlberg, R. G., et al. 1999, *ApJ*, 518, 533
- Maller, A. H., & Bullock, J. S. 2004, *MNRAS*, 355, 694
- Martin, C. L., & Bouché, N. 2009, *ApJ*, 703, 1394
- Martin, C. L., Shapley, A. E., Coil, A. L., et al. 2012, *ApJ*, 760, 127
- Nielsen, N. M., Churchill, C. W., & Kacprzak, G. G. 2012, *arXiv:1211.1380* (Paper II)
- Ocvirk, P., Pichon, C., Teyssier, R. 2008, *MNRAS*, 390, 1326
- Oppenheimer, B. D., Davé, R., Kereš, D., et al. 2010, *MNRAS*, 406, 2325
- Rao, S. M., Belfort-Mihalyi, M., Turnshek, D. A., et al. 2011, *MNRAS*, 416, 1215
- Rao, S. M., & Turnshek, D. A. 2000, *ApJS*, 130, 1
- Ribaudo, J., Lehner, N., Howk, J. C., et al. 2011, *ApJ*, 743, 207
- Rigby, J. R., Charlton, J. C., & Churchill, C. W. 2002, *ApJ*, 565, 743
- Rubin, K. H. R., Prochaska, J. X., Koo, D. C., & Phillips, A. C. 2012, *ApJ*, 747, L26
- Rubin, K. H. R., Weiner, B. J., Koo, D. C., et al. 2010, *ApJ*, 719, 1503
- Schneider, D. P., et al. 1993, *ApJS*, 87, 45
- Steidel, C. C. 1995, *QSO Absorption Lines*, 139
- Steidel, C. C., Dickinson, M., Meyer, D. M., Adelberger, K. L., & Sembach, K. R. 1997, *ApJ*, 480, 586 (Steidel97)
- Steidel, C. C., Dickinson, M., & Persson, S. E. 1994, *ApJ*, 437, L75 (SDP94)
- Steidel, C. C., Kollmeier, J. A., Shapley, A. E., et al. 2002, *ApJ*, 570, 526
- Steidel, C. C., & Sargent, W. L. W. 1992, *ApJS*, 80, 1
- Stewart, K. R., Kaufmann, T., Bullock, J. S., et al. 2011, *ApJ*, 738, 39
- Stoeck, J. T., Keeney, B. A., Danforth, C. W., et al. 2013, *ApJ*, 763, 148
- Thom, C., Werk, J. K., Tumlinson, J., et al. 2011, *ApJ*, 736, 1
- Tremonti, C. A., Moustakas, J., & Diamond-Stanic, A. M. 2007, *ApJ*, 663, L77
- Tumlinson, J., Thom, C., Werk, J. K., et al. 2011, *Science*, 334, 948
- van de Voort, F., Schaye, J., Booth, C. M., Haas, M. R., & Dalla Vecchia, C. 2011, *MNRAS*, 414, 2458
- van de Voort, F., & Schaye, J. 2012, *MNRAS*, 423, 2991
- Vogt, S. S., Allen, S. L., Bigelow, B. C., et al. 1994, *Proc. SPIE*, 2198, 362
- Wang, W., & Wells, M. T. 2000, *Statistica Sinica*, 10, 1199
- Weiner, B. J., Coil, A. L., Prochaska, J. X., et al. 2009, *ApJ*, 692, 187
- Werk, J. K., Prochaska, J. X., Thom, C., et al. 2013, *ApJS*, 204, 17
- Wolf, C., Meisenheimer, K., Rix, H.-W., et al. 2003, *A&A*, 401, 73
- Zibetti, S., Ménard, B., Nestor, D. B., Quider, A. M., Rao, S. M., & Turnshek, D. A. 2007, *ApJ*, 658, 161